HHS Public Access

Author manuscript

J Mol Biol. Author manuscript; available in PMC 2024 September 01.

Published in final edited form as:

J Mol Biol. 2023 September 01; 435(17): 168184. doi:10.1016/j.jmb.2023.168184.

J-domain proteins form binary complexes with Hsp90 and ternary complexes with Hsp90 and Hsp70

Anushka C. Wickramaratne[1,2], **Jui-Yun Liao**[1,2,8], **Shannon M. Doyle**[1,2,3], **Joel R. Hoskins**[1], **Gabrielle Puller**[1,4], **Madison L. Scott**[1], **John Paul Alao**[5], **Ikponwmosa Obaseki**[5], **Jerry C. Dinan**[6,7], **Tapan K. Maity**[6], **Lisa M. Jenkins**[6], **Andrea N. Kravats**[5,*], **Sue Wickner**[1,*]

[1]Laboratory of Molecular Biology, National Cancer Institute, National Institutes of Health, Bethesda, MD 20892, USA

[2]These people contributed equally

[3]Present address: National Institute of General Medical Sciences, National Institutes of Health, Bethesda, MD 20892, USA

[4]Present address: University of North Carolina, Chapel Hill, NC 27599

[5]Department of Chemistry and Biochemistry, Miami University, Oxford, OH 45056, USA

[6]Laboratory of Cell Biology, National Cancer Institute, National Institutes of Health, Bethesda, MD 20892, USA

[7]Present address: UT Southwestern Medical Center, Dallas, TX 75390, USA

[8]Present address: Department of Marine Biotechnology and Resources, National Sun Yat-sen University, Kaohsiung, Taiwan

Abstract

Hsp90 and Hsp70 are highly conserved molecular chaperones that help maintain proteostasis by participating in protein folding, unfolding, remodeling and activation of proteins. Both chaperones

*Correspondence to: Sue Wickner, 37 Convent Drive, Room 5144, NIH, Bethesda, MD 20892. wickners@mail.nih.gov; Andrea N. Kravats, Miami University, 132 Hughes Laboratories, 651 E. High St., Oxford, OH 45056, kravatan@MiamiOH.edu.

Author Contributions

A.C.W., J.R.L., S.M.D., J.R.H., G.C.P, M.L.S., A.N.K., L.M.J., and S.W. designed the experiments. A.C.W., J.R.L., S.M.D., J.R.H., G.C.P., J.P.C., I.O., M.L.S., J.C.D., T.K.M., L.M.J. and A.N.K. performed the experiments. All authors were involved in data interpretation and discussion. A.C.W., A.N.K. and S.W. wrote the manuscript with contributions from all other authors.

Competing Interest Statement

The authors declare no competing interests.

Declaration of interests

The authors declare that they have no known competing financial interests or personal relationships that could have appeared to influence the work reported in this paper.

CRediT author statement

A.C.W., J.R.L., S.M.D., J.R.H., G.C.P, M.L.S., A.N.K., L.M.J., and S.W.: Conceptualization, Methodology

A.C.W., J.R.L., S.M.D., J.R.H., G.C.P., J.P.C., I.O., M.L.S., J.C.D., T.K.M., L.M.J. and A.N.K.: Investigation

A.C.W., A.N.K. and S.W.: Writing – Review and Editing

Appendix A. Supplementary Material

are also important for cellular recovery following environmental stresses. Hsp90 and Hsp70 function collaboratively for the remodeling and activation of some client proteins. Previous studies using *E. coli* and *S. cerevisiae* showed that residues in the Hsp90 middle domain directly interact with a region in the Hsp70 nucleotide binding domain, in the same region known to bind J-domain proteins. Importantly, J-domain proteins facilitate and stabilize the interaction between Hsp90 and Hsp70 both in *E. coli* and *S. cerevisiae*. To further explore the role of J-domain proteins in protein reactivation, we tested the hypothesis that J-domain proteins participate in the collaboration between Hsp90 and Hsp70 by simultaneously interacting with Hsp90 and Hsp70. Using *E. coli* Hsp90, Hsp70 (DnaK), and a J-domain protein (CbpA), we detected a ternary complex containing all three proteins. The interaction involved the J-domain of CbpA, the DnaK binding region of *E. coli* Hsp90, and the J-domain protein binding region of DnaK where Hsp90 also binds. Additionally, results show that *E. coli* Hsp90 interacts with *E. coli* J-domain proteins, DnaJ and CbpA, and that yeast Hsp90, Hsp82, interacts with a yeast J-domain protein, Ydj1. Together these results suggest that the complexes may be transient intermediates in the pathway of collaborative protein remodeling by Hsp90 and Hsp70.

Graphical Abstract

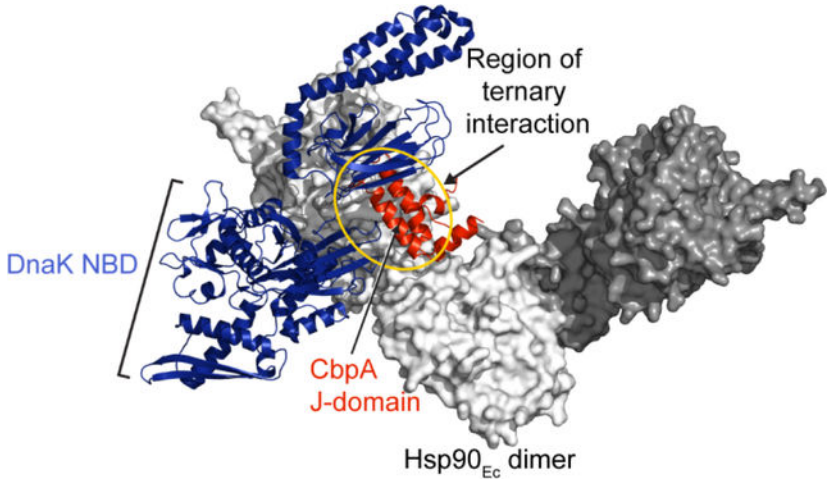

Docked model of an *E. coli* Hsp90-DnaK-CbpA complex

Keywords

molecular chaperones; DnaJ; Ydj1; Hsp82; HtpG

Introduction

Both Hsp90 and Hsp70 are ATP-dependent molecular chaperones that regulate the activity of hundreds of cellular proteins by remodeling and reactivating inactive proteins [1–4]. They are abundant proteins under nonstress conditions and are further induced by stress conditions [3, 5, 6]. Hsp90 is essential in all eukaryotes and in some bacteria, but not in *E. coli*, while Hsp70 is essential in all organisms [3–5, 7, 8]. Remodeling of many client proteins in both eukaryotes and bacteria requires the collaboration of Hsp90 and Hsp70 [3, 9–14].

Hsp90s are homodimers with each protomer composed of an N-terminal domain (NTD), a middle domain (MD), and a C-terminal domain (CTD) (Fig. 1a). In addition, eukaryotic Hsp90s have an unstructured linker of variable length connecting the N-domain to the M-domain, which bacterial Hsp90s lack [2, 3]. Cytoplasmic eukaryotic Hsp90s also have a C-terminal extension that is important for binding cochaperones containing tetratricopeptide repeat (TPR) domains [3, 15, 16]. The Hsp90 NTD binds ATP and, together with a catalytic loop in the MD, hydrolyzes ATP [2, 3]. A region in the MD of Hsp90 interacts with the Hsp70 chaperone, and the CTD facilitates Hsp90 dimerization [2, 3]. All Hsp90 domains are implicated in binding various clients [17]. The chaperone activity of Hsp90 requires ATP hydrolysis, which results in large conformational rearrangements that transform Hsp90 from an extended open conformation to a closed conformation characterized by transient dimerization at the NTDs and CTDs [18–20]. In eukaryotes, Hsp90 function is regulated by various combinations of more than twenty cochaperones, whereas bacteria lack Hsp90 cochaperone homologues [17, 21, 22].

Hsp70s are comprised of an N-terminal nucleotide-binding domain (NBD) and a C-terminal substrate-binding domain (SBD) that are connected by a short linker [1, 2] (Fig. 1b). The SBD is composed of two subdomains: SBDβ contains the substrate (client)-binding pocket and is composed of β-strands, and SBDα is a helical region that functions as a lid to cover the bound client. Similar to Hsp90, Hsp70 undergoes cycles of ATP binding and hydrolysis that are accompanied by large conformational changes in the chaperone [1, 2]. Hsp70 is regulated by two cochaperones, a J-domain proteins (JDP) and a nucleotide exchange factor (NEF). JDPs target specific substrate proteins to Hsp70 and stimulate Hsp70 ATP hydrolysis. There are three classes of JDPs, all containing a J-domain. Class A JDPs, such as *E. coli* DnaJ and yeast Ydj1, contain a J-domain followed by two homologous C-terminal domains referred to as CTD I and CTD II [23, 24]. They also contain a Zn^{2+} binding domain embedded in CTD I. Class B JDPs, such as *E. coli* CbpA and yeast Sis1, lack the Zn^{2+} binding domain but are otherwise homologous to type I JDPs. Class C JDPs contain a J-domain but are otherwise not homologous to JDPs. JDPs present substrates to Hsp70 and stimulate ATP hydrolysis by DnaK, causing high affinity substrate binding [1, 2]. NEFs trigger the release of ADP from Hsp70 and the binding of ATP, thereby promoting nucleotide exchange [25].

Physical interaction between bacterial Hsp90 and Hsp70 is required for Hsp90 and Hsp70 to synergistically function in client remodeling [4, 26]. Previously we demonstrated that direct interactions between *E. coli* Hsp90 ($Hsp90_{Ec}$) and Hsp70 (DnaK) and between *Saccharomyces cerevisiae* Hsp90 (Hsp82) and Hsp70 (Ssa1) are essential for client remodeling [9, 10, 13] (Fig. 1a). Residues in the MDs of both $Hsp90_{Ec}$ and Hsp82 are important for the Hsp90-Hsp70 interaction, and they directly contact residues in the NBDs of DnaK and Ssa1, respectively [12, 13, 27] (Fig. 1a). Moreover, many of the *E. coli* and yeast Hsp70 residues that are involved in Hsp90 binding were previously shown to be important for interaction with JDPs [12, 13] (Fig. 1b and 1c). It has also been observed that Hsp70-Hsp90 complex formation in the presence of ATP is stimulated by the addition of JDPs [10, 27]. The JDP likely stimulates the conversion of the ATP-bound conformation of Hsp70 to the ADP-conformation, which more readily interacts with Hsp90 [13, 27, 28]. In addition, the Hsp70-Hsp90 complex is stabilized by a known client protein, ribosomal

protein L2 [10]. Together, these results suggest that JDPs, Hsp70s, and Hsp90s function synergistically in protein remodeling.

In this work we explored the mechanism by which JDPs facilitate the collaboration between Hsp90 and Hsp70. Our results show that an *E. coli* JDP, CbpA, forms a ternary complex with Hsp90 and Hsp70. In addition, both *E. coli* and yeast J-domain proteins form binary complexes with Hsp90. These observations suggest that transient CbpA-$Hsp90_{Ec}$ complexes and CbpA-DnaK-$Hsp90_{Ec}$ complexes may be intermediates in the pathway of protein remodeling.

Results

Hsp90, Hsp70, and JDP form a ternary complex

Previous in vivo and in vitro research showed that there is a direct interaction between Hsp90 and Hsp70 [9, 10, 27]. It was also shown that the site of interaction between the two chaperones involved residues in the MD of Hsp90 and the NBD of Hsp70 [12]. Moreover, the residues in *E. coli* and yeast Hsp70 that interact with Hsp90 are also known to interact with JDPs [12, 13, 27, 29–32]. These observations suggested the possibility that Hsp90 and JDP compete for binding Hsp70. However, CbpA and DnaJ did not compete with $Hsp90_{Ec}$ in pull-down assays with biotin labeled DnaK (Genest 2015). Similarly, *E. coli* and yeast JDPs did not compete with *E. coli* and yeast Hsp70s in Hsp70-Hsp90 crosslinking experiments. Instead, *E. coli* and yeast JDPs facilitated or stabilized the Hsp90-Hsp70 complex in the presence of client and ATP (Genest, 2015, Doyle 2019). These results suggested the possibility that JDPs may form a larger Hsp90-Hsp70-JDP complex as a transient intermediate in the pathway of client remodeling. To test this hypothesis, we performed crosslinking experiments using a trifunctional crosslinker, TMEA (tris(2-meleimidoethyl)amine), containing three reactive maleimide groups with linker lengths of 10.3 Å, to enable conjugation to sulfhydryl-containing molecules. We constructed cysteine substitution mutants in $Hsp90_{Ec}$, DnaK, and CbpA, since $Hsp90_{Ec}$ and CbpA lack cysteines and DnaK contains one buried cysteine that does not interfere in crosslinking experiments [27]. The residues selected for mutation were nearby the known $Hsp90_{Ec}$-DnaK and the DnaK-DnaJ interfaces (Fig. 1). After testing various mutants, we focused on the combination of $Hsp90_{Ec}$ N347C, CbpA E51C and DnaK D211C (Fig. 2a, 2b). All three of the mutant proteins function like their wild type counterparts in protein reactivation and ATP hydrolysis (Fig. S1, [27]).

The $Hsp90_{Ec}$, DnaK, and CbpA cysteine mutant proteins were incubated individually, in pairs, and all three together in the presence of TMEA and ATP. The rationale for including ATP was to allow the chaperones to undergo conformational changes that may be necessary for formation of a transient complex. The crosslinked products were then visualized by SDS-PAGE. Strikingly, a novel, slowly migrating species was observed when $Hsp90_{Ec}$ N347C, CbpA E51C and DnaK D211C were crosslinked (Fig. 2c, lane 7), but not when any one of the three components was omitted (Fig. 2c, lanes 4–6). When wild-type $Hsp90_{Ec}$, DnaK, or CbpA was substituted in the reaction for the corresponding cysteine mutants, the high molecular weight crosslinked product was not observed, indicating that the crosslinked complex consists of the three cysteine mutants of $Hsp90_{Ec}$, DnaK and CbpA (Fig. 2c, lanes

8–10). When either $Hsp90_{Ec}$ or CbpA alone was treated with TMEA, a small amount of crosslinked $Hsp90_{Ec}$ protomers or CbpA protomers could be seen (Fig. 2c, lanes 1 and 3). When DnaK alone was treated with TMEA, crosslinked DnaK protomers were not detected (Fig. 2c, lane 2). DnaK and CbpA crosslinked as expected (Fig. 2c, lane 4) as did DnaK and $Hsp90_{Ec}$, (Fig. 2c, lane 6). Interestingly, we also observed a new crosslinked species when $Hsp90_{Ec}$ and CbpA were treated with TMEA in the absence of DnaK, suggesting a binary complex of $Hsp90_{Ec}$ and CbpA (Fig. 2c, lane 5). This observation was pursued in greater detail in sections below. In control experiments, in the absence of crosslinker, the expected protomer species were seen, but not higher slowly migrating species (Fig. S2a). Together these results demonstrate a novel potential ternary complex comprised of $Hsp90_{Ec}$, CbpA, and DnaK.

We next tested the effect of nucleotides on the formation of the new complex by performing TMEA crosslinking in the absence of nucleotide or in the presence of ATP, ADP or AMP-PNP (Fig. 2d, S2b–d). Similar amounts of new complex were observed with all conditions. These observations show that formation of the potential ternary complex is independent of nucleotide, suggesting the closed or open conformations of DnaK and $Hsp90_{Ec}$ can participate in ternary complex formation.

To address whether ATP binding by the chaperones was important for formation of the new complex we performed crosslinking experiments using previously characterized Hsp90Ec and DnaK mutants that are defective in ATP binding. Starting with $Hsp90_{Ec}$ D80N [33, 34] and DnaK K70A [35] mutants that are deficient in ATP binding, we constructed double mutants, $Hsp90_{Ec}$ N347C/D80N and DnaK D211C/K70A, for crosslinking (Fig. S1i, j). When the double mutants were tested in crosslinking experiments using TMEA, we observed formation of the new complex, both with and without ATP (Fig. 2e, 2f). Thus, formation of the new slowly migrating species can occur independent of ATP binding and hydrolysis by $Hsp90_{Ec}$ and DnaK.

Characterization of the $Hsp90_{Ec}$-DnaK-CbpA complex

To determine the composition of the potential ternary complex, TMEA crosslinking followed by mass spectrometry (MS) analysis was performed. The TMEA crosslinking experiment compared a sample with all three proteins to samples where pairs of proteins were incubated with TMEA (Fig. 3a). Following SDS-PAGE, MS analysis of the band containing the slow migrating potential ternary complex confirmed the presence of all three proteins (Fig. 3a (sample A), Fig. 3b). In control experiments containing pairs of proteins, MS analysis of the region of the gel where the ternary complex migrated detected background levels of the two proteins present in the pair (Fig. 3a (samples B-D), Fig. 3b). The TMEA experiment was repeated with a sample containing all three proteins together with TMEA and the analysis confirmed the presence of all three proteins (Fig. S3).

To further define the sites of interactions among the three proteins, we monitored the ability of various $Hsp90_{Ec}$ mutants to participate in ternary complex formation using TMEA crosslinking. $Hsp90_{Ec}$ N350C, which is near N347 in the DnaK binding region of $Hsp90_{Ec}$ and has properties like wild type (Fig. 2a, S1a–d), formed a prominent ternary complex (Fig. 4a, lanes 1 and 2). Ternary complexes were faintly visible or not visible when $Hsp90_{Ec}$

mutants defective in protein reactivation and in DnaK binding [10, 27], including $Hsp90_{Ec}$ K354C, Q358C, K238C, R267C, E269C, and R355C, were incubated with DnaK, CbpA and TMEA (Fig. 4a, lanes 3–8). As expected, the ternary complex was not observed when L493C, a residue in the Hsp90 C-terminal domain (CTD), was used in the crosslinking reaction (Fig. 4a, lane 9). These observations suggest that the residues important for $Hsp90_{Ec}$-DnaK complex formation are also important for ternary complex formation or that the residues tested are too far away from DnaK in the ternary complex to form crosslinks.

Additional cysteine mutants in helices 2 and 3 of the CbpA J-domain were also constructed and tested for ability to form ternary complexes (Fig. 2b). All of the mutants, K22C, A44C, and S57C, had properties similar to wild type (Fig. S1e–g) and formed ternary complexes when treated with TMEA in the presence of $Hsp90_{Ec}$ N347C and DnaK D211C, although K22C was slightly defective compared to the other mutants (Fig. 4b, lanes 1–4). CbpA S295C, a mutant in the CTD II, did not form the ternary species, as expected (Fig. 4b, lane 5). These observations show that the region of CbpA involved in ternary complex formation involves both helix 2 and helix 3 of the J-domain. Taken together, these results suggest that the NBD of DnaK simultaneously interacts with the MD of $Hsp90_{Ec}$ and the J-domain of CbpA to form an $Hsp90_{Ec}$-DnaK-CbpA ternary complex.

To test if the CbpA J-domain was sufficient for ternary complex formation with $Hsp90_{Ec}$ and DnaK, we constructed and purified a CbpA J-domain fragment (residues 1–78 [36]) containing a cysteine substitution in residue A44C (CbpA J-domain A44C). We tested its ability to form a crosslinked species with $Hsp90_{Ec}$ N347C and DnaK D211C when treated with TMEA (Fig. 4c). A new species migrating slightly slower than $Hsp90_{Ec}$-DnaK complexes was seen (Fig. 4c, lane 7), consistent with a complex containing the CbpA J-domain fragment, $Hsp90_{Ec}$ and DnaK. The new higher molecular weight product was not observed when wild-type CbpA J-domain, $Hsp90_{Ec}$, or DnaK was substituted in the reaction mixture for the corresponding cysteine mutant (Fig. 4c, lanes 8–10). Binary complexes of DnaK-CbpA J-domain and $Hsp90_{Ec}$-CbpA J-domain were also observed (Fig. 4c, lanes 4–5). In another control, when the CbpA J-domain was incubated alone with TMEA, no band was observed in the position of the potential new complex (Fig. 4c, lane 3). Western blot analysis of the gel after TMEA crosslinking confirmed that the new species contained the CbpA J-domain (Fig. 4d, Fig. S4). These results demonstrate that the J-domain fragment of CbpA is sufficient for ternary complex formation with $Hsp90_{Ec}$ and DnaK.

Direct interactions between Hsp90s and J-domain proteins

As mentioned earlier, we observed an interaction between $Hsp90_{Ec}$ and CbpA in the absence of DnaK while investigating the $Hsp90_{Ec}$-DnaK-CbpA complex (Fig. 2c, lane 5). A similar observation was previously reported showing that *Synechococcus elongatus* Hsp90 and *S. elongatus* DnaJ2, a type II JDP, interact [37]. In addition, the DnaJ2 CTD I and II were found to be involved in the interaction. To further explore the *E. coli* $Hsp90_{Ec}$-CbpA interaction, we performed pull-down assays using $Hsp90_{Ec}$ and biotin-labeled CbpA. We found that $Hsp90_{Ec}$ associated with CbpA in a concentration-dependent manner, thus confirming a physical interaction between the two proteins (Fig. 5a–5d). In the presence of ATP, ~50% less $Hsp90_{Ec}$ associated with CbpA than in the absence of ATP (Fig. 5a,

5b). Similarly, decreased $Hsp90_{Ec}$ association with CbpA was also observed in the presence of AMP-PNP or ADP (Fig. S5a–d). The addition of a client protein, ribosomal protein L2, resulted in approximately four-fold more $Hsp90_{Ec}$ associated with CbpA-biotin (Fig. 5c, 5d). These results suggest that the open conformation of $Hsp90_{Ec}$ favors interaction with CbpA and the client protein stabilizes the interaction between CbpA and $Hsp90_{Ec}$ (Fig. 5e). No effect of CbpA on the $Hsp90_{Ec}$ ATPase activity in the presence or absence of L2 was detected (Fig. S5e).

We also tested if DnaJ, a type I JDP and the major *E. coli* JDP, could interact with $Hsp90_{Ec}$. Using biotin-labeled DnaJ, we observed that DnaJ, like CbpA, associated with $Hsp90_{Ec}$ in pull-down assays (Fig. 6a–6d). About 50% less $Hsp90_{Ec}$-DnaJ complex was observed in the presence of ATP than in the absence of ATP and ~50% more in the presence of L2 than in the absence of L2 (Fig. 6a–6d). The presence of ADP or AMP-PNP similarly resulted in decreased $Hsp90_{Ec}$-DnaJ interaction, suggesting the open form of $Hsp90_{Ec}$ is the slightly preferred conformation for DnaJ binding (Fig. 6e, Fig. S6a–d). Interactions between the two JDPs and $Hsp90_{Ec}$ were additionally monitored using BioLayer Interferometry (BLI), which revealed a modest affinity of Hsp90 for JDP. In the absence of ATP, the K_d values for DnaJ-$Hsp90_{Ec}$ and CbpA-$Hsp90_{Ec}$ complexes were 3.6 ± 0.3 μM and 11 ± 0.9 μM, respectively (Fig. 5f, 6f, Fig. S7a–d). Thus, these results demonstrate that both type I and type II *E. coli* JDPs interact directly with $Hsp90_{Ec}$.

To determine if the interaction between Hsp90 and JDP is conserved across species, pull-down assays using *S. cerevisiae* Hsp90 (Hsp82) and biotin-labeled Ydj1, a yeast type I JDP, were performed. Hsp82 associated with Ydj1 and the interaction was slightly inhibited when ATP, ADP, or AMP-PNP was present and was stimulated approximately two-fold by L2 (Fig. 7a–e, Fig. S6e–h). As seen with CbpA, there was no detectable effect of Ydj1 on the Hsp82 ATPase activity (Fig. S5f). The Hsp82-Ydj1 complex was also monitored using BLI, showing a K_d of 3 ± 0.2 μM (Fig. 7f, Fig. S7e, S7f). Altogether, the results show that Hsp90s and JDPs physically interact and highlight the conserved nature of the interaction between bacteria and yeast.

Identification of $Hsp90_{Ec}$ and CbpA interaction sites

Based on our findings that Hsp90 and JDPs directly interact, we next sought to determine the sites on $Hsp90_{Ec}$ and CbpA involved in the interaction. Crosslinking between $Hsp90_{Ec}$ and CbpA in the absence of ATP using disuccinimidyl sulfoxide (DSSO), an amine-reactive crosslinker with a 10.3 Å spacer arm followed by tandem mass spectrometry (XL-MS) was utilized to assess intermolecular interactions in an unbiased manner. Numerous crosslinks were observed between the two proteins. Residues in the J-domain of CbpA crosslinked with residues in the NTD, MD, and CTD of $Hsp90_{Ec}$ (Fig. 8a–c, Fig. S8a, S8b). Additionally, CbpA CTD I and CTD II crosslinks with the $Hsp90_{Ec}$ MD and CTD, respectively, were observed. These results suggest that there are multiple possible CbpA binding sites on $Hsp90_{Ec}$ and suggest that multiple CbpA protomers may contact $Hsp90_{Ec}$ simultaneously.

Interaction between the $Hsp90_{Ec}$ DnaK binding region and CbpA

We further explored the interaction between the MD of $Hsp90_{Ec}$ and CbpA observed in the XL-MS experiment. This region was of particular interest because the two $Hsp90_{Ec}$ MD residues, K238 and K354, that interacted with CbpA in the XL-MS experiment (Fig. 8a) were previously shown to be important for protein reactivation by the collaborative activity of $Hsp90_{Ec}$, DnaK, and DnaK cochaperones, and for the direct interaction with DnaK [10, 13, 27]. Additionally, this region of $Hsp90_{Ec}$ was shown above to be involved in ternary complex formation with DnaK and CbpA (Fig. 4a).

To confirm that CbpA forms a binary complex with $Hsp90_{Ec}$ through residues overlapping the DnaK binding site, we used cysteine-specific crosslinking. Interactions between $Hsp90_{Ec}$ K238C and CbpA K22C as well as between $Hsp90_{Ec}$ K354C and CbpA K22C were probed using bis(maleimido)ethane (BMOE), a homobifunctional cysteine reactive crosslinker with a spacer arm of 8.0 Å. CbpA K22C was chosen since it was identified as a residue involved in XL-MS that crosslinked with both $Hsp90_{Ec}$ K238C and K354C (Fig. 8a). In addition, it has properties like wild type (Fig. S1e–f) and forms ternary complexes with $Hsp90_{Ec}$ and DnaK (Fig. 4b). Following treatment with crosslinker in the absence of ATP, we observed that both $Hsp90_{Ec}$ K238C and K354C produced a higher molecular weight product when incubated with CbpA K22C (Fig. 8d, lanes 5 and 6). When $Hsp90_{Ec}$ K238C, $Hsp90_{Ec}$ K354C, or CbpA K22C alone was treated with crosslinker, the potential $Hsp90_{Ec}$-CbpA species was not observed (Fig. 8d, lanes 2, 3 and 4, Fig. S8c).

To validate the presence of $Hsp90_{Ec}$ and CbpA in the BMOE crosslinked species, the experiment was repeated using a reversible homobifunctional, cysteine-reactive crosslinker, dithiobismaleimidoethane (DTME). The crosslinked species formed with $Hsp90_{Ec}$ K238C or K354C and CbpA K22C migrated similarly on SDS-PAGE to those obtained with BMOE (Fig. 8e, Fig. S8d). The potential $Hsp90_{Ec}$-CbpA crosslinked species were extracted from the gel, treated with a reducing agent, and analyzed by SDS-PAGE. Approximately equal amounts of $Hsp90_{Ec}$ and CbpA were observed with either $Hsp90_{Ec}$ mutant (Fig. 8e, lanes 2 and 4). These results confirm that residues in the DnaK binding region of $Hsp90_{Ec}$ directly interact with the J-domain of CbpA.

We next tested four $Hsp90_{Ec}$ mutants that are defective or partially defective in binding DnaK, including K354C, R355C, Q358C, and a double mutant G270A/K271A (Fig. 2a) [10], for their ability to bind CbpA using pull-down assays in the absence of ATP and the presence of L2. Two $Hsp90_{Ec}$ mutants, R355C and G270A/K271A, were defective in interaction with biotinylated CbpA (Fig. 9a, 9b, S9a). The other two $Hsp90_{Ec}$ mutants, K354C and Q358C, bound CbpA like wild type (Fig. 9a, 9b, S9a). $Hsp90_{Ec}$ N347C and N350C, that bind DnaK like wild type and participate in ternary complex formation (Fig. 4a, Fig. S1c, S1d), also bound CbpA similar to wild type (Fig. 9a, 9b). An $Hsp90_{Ec}$ mutant in the CTD, L493C, which is far from the DnaK binding region, also bound CbpA like wild type (Fig. 9a, 9b, Fig. S9a). We next tested yeast Hsp82 mutants that are defective in Ssa1 interaction [13] (Fig. 9c) for their ability to interact with Ydj1 in pull-down assays in the absence of ATP. We observed that Hsp82 G313S and K398E, which are homologous to $Hsp90_{Ec}$ G270 and K354, respectively, were defective in interaction with Ydj1 compared to wild type (Fig. 9c–e, Fig. S9b). Substitution mutants in two other residues in the Ssa1

binding region of Hsp82, K394C and K399C, were not defective. These results show that the region of Hsp90 that interacts with JDP overlaps with the region that interacts with Hsp70 and is conserved between *E. coli* and yeast.

BMOE crosslinking was also used to probe the interaction between the DnaK binding region of $Hsp90_{Ec}$ and CbpA. We tested several $Hsp90_{Ec}$ cysteine mutants in the MD region that are defective in binding DnaK [10] for their ability to crosslink to CbpA E51C (Fig. S10a, S10b). We observed more mutants to be partially defective in $Hsp90_{Ec}$-CbpA interaction using the crosslinking technique compared to the pull-down assay. The differences possibly reflect differences in the assays, since all three $Hsp90_{Ec}$ domains can participate in the pull-down assay while only one cysteine mutant at a time can participate in the crosslinking assay. Crosslinking also has the additional constraint that the cysteine mutants must be close enough to form the crosslink necessary to capture complex formation. Altogether, both pull-down and crosslinking results demonstrate that the DnaK binding region of $Hsp90_{Ec}$ is important for the interaction with CbpA.

We also tested several other cysteine substitutions in the CbpA J-domain for their ability to interact with the $Hsp90_{Ec}$ MD in crosslinking experiments (Fig. 10a, Fig S10c). All of the CbpA J-domain mutants, including K22C, A44C, and S57C, interacted with $Hsp90_{Ec}$ N347 similarly to CbpA E51C. In a control, crosslinking was very weak between $Hsp90_{Ec}$ N347C and CbpA S295C, a residue in the dimerization domain of CbpA (Fig. 10a, Fig. S10c). The results show that multiple residues in in the CbpA J-domain can interact with the DnaK binding region of $Hsp90_{Ec}$. They also show that the same CbpA J-domain residues that are involved in forming ternary complexes with DnaK and $Hsp90_{Ec}$ are also involved in forming binary complexes with $Hsp90_{Ec}$.

To determine if the J-domain alone was sufficient to carry out the observed interaction between CbpA and the $Hsp90_{Ec}$ MD, we tested if the CbpA J-domain A44C fragment was able to form a crosslinked species with $Hsp90_{Ec}$ using BMOE. This binary $Hsp90_{Ec}$-CbpA J-domain complex was previously observed using TMEA crosslinking (Fig. 4c, lane 5, 4d). When either $Hsp90_{Ec}$ N347C or N350C was crosslinked with the CbpA J-domain, a new higher molecular weight species, consistent with a complex of the J-domain and $Hsp90_{Ec}$, was observed (Fig. 10b, lanes 6 and 7). The new higher molecular weight product was not observed when CbpA J-domain A44C was incubated with $Hsp90_{Ec}$ R355C or L493C and BMOE (Fig 10b, lanes 8 and 9). These results reflect the specificity of the binary complex formed with full-length CbpA E51C and the corresponding $Hsp90_{Ec}$ mutants (Fig. S10a, S10b). When CbpA J-domain A44C alone was treated with crosslinker, the higher molecular weight complex was not observed (Fig 10b, lane 5). Similarly, addition of the wild-type CbpA J-domain fragment to crosslinking assay with CbpA E51C and $Hsp90_{Ec}$ N347C disrupted the CbpA-$Hsp90_{Ec}$ interaction in a concentration-dependent manner (Fig. S10d, S10e). Together these results show the ability of the CbpA J-domain to interact with the DnaK binding region of $Hsp90_{Ec}$ independently of the substrate binding domains CTD I and CTD II.

Interactions between the $Hsp90_{Ec}$ N-terminal domain and CbpA and between the $Hsp90_{Ec}$ C-terminal domain and CbpA

We further explored the interactions between the other domains of $Hsp90_{Ec}$ and CbpA that were identified by DSSO XL-MS (Fig. 8a). We constructed cysteine substitutions in the five $Hsp90_{Ec}$ NTD residues identified by XL-MS, including K45C, K71C, K99C, K103C, and K199C (Fig. 8b). All five $Hsp90_{Ec}$ NTD mutants reactivated denatured proteins with DnaK, CbpA and GrpE similarly to wild type (Fig. S11). When tested in crosslinking experiments with CbpA K22C using BMOE, all of the $Hsp90_{Ec}$ NTD mutants exhibited slower migrating species, consistent with $Hsp90_{Ec}$-CbpA complexes, that were not observed when the $Hsp90_{Ec}$ NTD mutants were treated with BMOE in the absence of CbpA (Fig. 11a). We tested if wild type CbpA J-domain fragment (residues 1–78) [36] could inhibit crosslinking between $Hsp90_{Ec}$ K199C and CbpA E51C by competition and observed that increasing concentrations of CbpA J-domain fragment led to a decrease in the $Hsp90_{Ec}$-CbpA crosslinked species (Fig. 11b–11c, Fig. S12a). Similar results were observed when full-length CbpA wild type was used as a competitor (Fig. 11b–11c, Fig. S12a). These results suggest that the CbpA J-domain is largely responsible for the interaction between CbpA and the $Hsp90_{Ec}$ K199C.

To test if the region of DnaK that interacts with CbpA and the $Hsp90_{Ec}$ MD could alternatively interact with CbpA and the $Hsp90_{Ec}$ NTD, we carried out TMEA crosslinking experiments with DnaK D211C, CbpA E51C, and each of the five $Hsp90_{Ec}$ NTD cysteine mutants. Ternary complexes were not observed (Fig. S12b, S12c). Lastly, in pull-down assays, $Hsp90_{Ec}$ K45C, K71C, K103C and K199C were similar to wild type in their ability to interact with biotinylated CbpA in the presence of L2 and the absence of ATP, while K99C interaction with CbpA was slightly defective (Fig. S12d, S12e, S9c). These results suggest that the $Hsp90_{Ec}$ NTD is important for interaction with CbpA.

We also constructed cysteine substitution mutants in the $Hsp90_{Ec}$ CTD residues identified by XL-MS (Fig. 8a–b). The mutants, $Hsp90_{Ec}$ K492C, K502C and K560C, exhibited properties like wild type in protein reactivation assays and ATPase assays (Fig. S13). When tested in pull-down assays with biotinylated CbpA in the absence of ATP and the presence of L2, they bound CbpA similarly to wild type (Fig. S13, Fig. S9d). Together the results show that all three domains of $Hsp90_{Ec}$ are capable of binding CbpA, although only the MD interactions are essential for protein reactivation.

Discussion

The results presented here demonstrate that $Hsp90_{Ec}$, DnaK, and CbpA simultaneously interact through the DnaK binding region in the middle domain of $Hsp90_{Ec}$, the DnaJ binding region of DnaK, and the J-domain of CbpA. Additionally, the results show binary complexes between both *E. coli* and yeast Hsp90s and JDPs.

We used molecular modeling to visualize the possible arrangement of $Hsp90_{Ec}$, DnaK, and CbpA in a complex that allowed the three proteins to contact one another through residues determined experimentally. The closed form of DnaK (PDB ID 2KHO [38]) was used because the ternary complex forms with a DnaK mutant deficient in ATP binding (Fig. 2f).

The NBD of DnaK (residues 1–390) was used because this domain of DnaK was observed to crosslink with $Hsp90_{Ec}$ and CbpA (Fig. 2). The open form of $Hsp90_{Ec}$ (PDB ID 2IOQ [39]) was used since an $Hsp90_{Ec}$ mutant defective in ATP binding was able to form ternary complexes (Fig. 2e). It is also the form known to interact with DnaK [12, 28]. The J-domain of CbpA (PDB ID 2KQX [40]) was used because our results showed the J-domain was sufficient for complex formation (Fig 4c, 4d). Distance restraints were incorporated based on the TMEA crosslinking data (Fig. 2c and Fig. 4a, 4b, and Table S1; see Materials and Methods for modeling procedure). The resulting models were sorted based on their docking scores and the standard deviation for each model was considered. Complexes with clashes with the second protomer of the $Hsp90_{Ec}$ dimer were eliminated. The complex with the best score, lowest interface RMSD, and largest number of clustered models (Fig. S14) is presented in Fig. 12a, while the second model is presented in Fig. S15a. Importantly, the models show it is feasible for CbpA, DnaK and $Hsp90_{Ec}$ to contact one another in a ternary complex. Most observed distances of the experimentally determined residues in the modeled ternary complexes are within the 10.3 Å crosslinker spacer arm restraint (Fig. S14c).

In the top ternary model (Fig. 12a), the orientation of the DnaK NBD is compatible with the full-length ADP bound DnaK molecule (Fig. 12b). Interestingly, this orientation of DnaK relative to $Hsp90_{Ec}$ is similar to the orientation of ADP-bound DnaK in the docked model of the binary DnaK-$Hsp90_{Ec}$ complex (Fig. 12c) [12]. In the ternary model, the CbpA J-domain contacts DnaK in the general vicinity where the DnaJ J-domain contacts DnaK in the DnaK-DnaJ-domain cocrystal; however, it is rotated ~45° and shifted to interact with the opposite face of DnaK subdomain IIA compared to the DnaK-DnaJ-domain cocrystal (Fig. 12d). Analysis of the second model indicates compatibility with the full-length ADP-bound DnaK structure but shows inconsistencies with binary DnaK-$Hsp90_{Ec}$ and DnaK-DnaJ J-domain complexes (Fig. S15). Together, the modeling shows that ternary complexes comprised of CbpA, $Hsp90_{Ec}$ and DnaK are plausible.

Molecular docking was also used to visualize the CbpA J-domain interaction with the $Hsp90_{Ec}$ MD. For modeling, the apo form of $Hsp90_{Ec}$ (PDB ID 2IOQ [39]) was used because the best experimental condition to detect complex formation was in the absence of nucleotide (Fig. 5, Fig. S5). The CbpA J-domain structure (PDB ID 2KQX [40]) was used since residues in the J-domain crosslinked with the $Hsp90_{Ec}$ MD (Fig. 10b) and because the CbpA J-domain competed with full-length CbpA for $Hsp90_{Ec}$ binding (Fig. 11b and 11c). The docked binary J-domain-$Hsp90_{Ec}$ model with the most favorable docking score is shown in Fig. 12e (Materials and Methods; Fig. S16). The J-domain is in the general vicinity of $Hsp90_{Ec}$ where it is observed in the top ternary models (Fig. 12a). However, alignment of the binary $Hsp90_{Ec}$-CbpA model and the ternary $Hsp90_{Ec}$-DnaK-CbpA model with respect to $Hsp90_{Ec}$ shows that the CbpA J-domain in the ternary complex is shifted and rotated (Fig. 12f, S15e).

A “working model” for the mechanism of protein reactivation by bacterial Hsp90, DnaK, and CbpA is shown in Fig. 13. While many aspects are speculative, it provides a framework for further investigation. Likely, the client protein binds CbpA and is targeted to DnaK. Cycles of client binding and release from DnaK, facilitated by GrpE, promote partial client refolding (Fig. 13, step 1). Next, DnaK, CbpA and client may interact with the MD of

$Hsp90_{Ec}$, forming a transient quaternary $Hsp90_{Ec}$-DnaK-CbpA-client complex (Fig. 13, step 2). While in the transient complex the client may be transferred from DnaK to $Hsp90_{Ec}$ as DnaK and CbpA dissociate (Fig. 13, step 3). It is possible that the order of dissociation of CbpA and DnaK from the quaternary complex is not specific; either one can leave first. This possibility is consistent with the observations that $Hsp90_{Ec}$ binds CbpA (Fig. 5) and DnaK [12] with similar affinities. In the last step of the working model, the client is released from $Hsp90_{Ec}$ and refolds in its active conformation (Fig. 13, step 4). The current data are also consistent with the possibility that the CbpA-$Hsp90_{Ec}$-client complex recruits DnaK to form a quaternary $Hsp90_{Ec}$-DnaK-CbpA-client intermediate. Although ATP hydrolysis is required for protein remodeling by the Hsp70 system alone and by collaborative function of Hsp90 and the Hsp70 system, it is not required for formation of the Hsp90-JDP and $Hsp90_{Ec}$-DnaK-CbpA complexes described here or for the Hsp90-Hsp70 complex. It is clear further research will be necessary to dissect out the pathway of the protein refolding by this complicated multichaperone system and to identify the steps requiring ATP hydrolysis.

In contrast to protein remodeling facilitated by bacterial Hsp90 and Hsp70 chaperones, the process in eukaryotes in significantly more complex. However, some underlying principles may be similar. Recent work by Agard and colleagues using human chaperones captured an Hsp90 ‘client loading’ complex for a model client, glucocorticoid receptor (GR) by cryo-electron microscopy [41]. The complex consists of an Hsp90 dimer, two Hsp70s, the cochaperone Hop (Hsp90/Hsp70 organizing protein), and GR. One portion of GR is bound in the SBD of Hsp70 and another is bound in the Hsp90 lumen. The NBD of Hsp70 is bound to the MD of Hsp90 and interacts through a homologous interface as shown for the DnaK-$Hsp90_{Ec}$ interaction [12]. Similar to our previous observations in the bacterial chaperone system, the ATP conformations of Hsp70 and Hsp90 are incompatible with complex formation in the eukaryotic chaperone system. In the resolved eukaryotic client loading complex, the second Hsp70 molecule is bound to the other Hsp90 protomer and serves a scaffolding role in complex formation, while Hop interacts with Hsp70, Hsp90, and GR. For client remodeling to occur, Hsp90 transitions from the transient client loading complex to a closed conformation and hydrolyzes ATP. At the same time, Hsp70 and Hop dissociate, and the cochaperone p23 binds to Hsp90 and GR, forming the ‘maturation complex’ [42]. Alternative remodeling pathways without the direct transient Hsp90-Hsp70 interaction have also been observed, suggesting that multiple pathways likely exist for client delivery to Hsp90. Recently, a mechanism for the transfer of GR from human Hsp70 to Hsp90 was discovered by Buchner and colleagues [43]. They found that an Hsp90 cochaperone, NudC, functions in the transfer of the client from Hsp40-Hsp70-client complexes to Hsp90. By interacting with JDP and Hsp90, NudC transfers the client from Hsp70 to Hsp90, bypassing the requirement for a direct Hsp90-Hsp70 interaction in client transfer. Together, these studies have shown that the formation of large chaperone complexes for client remodeling in eukaryotes requires participation of numerous Hsp90 cochaperones. Additional complexity in eukaryotic systems is introduced by post translational modifications that further regulate cochaperone binding and client remodeling by Hsp90 [44]. Thus, while bacteria, like eukaryotes, use two major chaperones, Hsp70 and Hsp90, in protein remodeling reactions, the regulation of collaboration between Hsp70 and Hsp90 differ. Collaboration between bacterial Hsp90 and Hsp70 relies on weak and transient interactions between Hsp90, Hsp70

and JDP, while eukaryotes have evolved to use Hsp90 cochaperones to mediate the coupling between Hsp90 and Hsp70. Further work is necessary to establish the function of these complexes in chaperone-mediated protein remodeling.

Materials and Methods

Plasmids and Proteins

Site-directed substitution mutants $Hsp90_{Ec}$ N347C, N350C, K45C, K71C, K99C, K103C, K199C, L493C, K492C, K502C, K560C, N347C/D80N; CbpA K22C, A44C, E51C, S57C, S295C; CbpA J-domain fragment A44C; and DnaK D211C/K70A were made with the QuikChange Lightning mutagenesis system (Agilent 210519–5) using pET-HtpG [9], pET-CbpA and pET-CbpA(1–78) [36]. pET-CbpA was constructed by generating a *cbpA* PCR fragment from *E. coli* DH5, containing 5' and 3' NdeI and HindIII sites, respectively. The PCR fragment was digested with NdeI and HindIII and ligated into similarly digested pET24b. All mutations were verified by DNA sequencing. $Hsp90_{Ec}$ K354C, Q358C, K238C, R267C, E269C, R355C, and G270A/K271A were previously constructed as described [10]. DnaK D211C [27], E209C [12], G238C [27] were previously constructed as described.

$Hsp90_{Ec}$ wild-type and mutants [9], DnaK wild-type and mutants [45], CbpA wild-type and mutants [46], CbpA J-domain wild-type and mutant [36], Hsp82 wild-type and mutants [13, 47], Ydj1 [48, 49], and His-tagged L2 [50] were isolated as described. All proteins were >95% pure as determined by SDS-PAGE. Luciferase (E1701) and luciferin (E1603) were from Promega. Concentrations given are for $Hsp90_{Ec}$, Hsp82, CbpA, and Ydj1 dimers and DnaK, L2, and luciferase monomers. Newly constructed $Hsp90_{Ec}$ and CbpA mutant proteins were characterized. All were found to coelute in size exclusion column chromatography like the wild-type. ATP hydrolysis rates were determined for the $Hsp90_{Ec}$ mutants and both $Hsp90_{Ec}$ and CbpA mutants were tested in protein reactivation assays.

Crosslinking

TMEA (tris(2-maleimidoethyl)amine, Thermo Fisher 33043) crosslinking reactions (25 μL) contained TKME Buffer, 4 mM ATP (unless indicated otherwise), 5 mM $MgCl_2$, 2 μM $Hsp90_{Ec}$, 2 μM DnaK, and 2 μM CbpA cysteine mutants and/or wild-type proteins as indicated. Proteins were crosslinked in the presence of 0.4 mM TMEA at 23 °C for 1 hr, quenched with 40 mM DTT at 23 °C for 15 min, and analyzed by Coomassie staining following SDS-PAGE.

DSSO (disuccinimidyl sulfoxide, Thermo Fisher A33545) crosslinking reactions (25 μL) contained 20 mM Hepes, 75 mM KCl, 10 mM $MgCl_2$, and 7 μM $Hsp90_{Ec}$ and 14 μM CbpA wild-type. Proteins were crosslinked in the presence of 0.19 mM DSSO at 23 °C for 30 min with mixing and analyzed by Coomassie staining following SDS-PAGE.

BMOE (bismaleimidoethane, Thermo Fisher 22323) crosslinking reactions (25 μL) contained TKME Buffer, 2 μM $Hsp90_{Ec}$ and 2 μM CbpA cysteine mutants as indicated. Proteins were crosslinked in the presence of 0.4 mM BMOE at 23 °C for 1 hr, quenched with 40 mM DTT at 23 °C for 15 min, and analyzed by Coomassie staining following SDS-PAGE.

DTME (dithiobismaleimidoethane, Thermo Fisher 22335) crosslinking reactions (25 μL) contained 20 mM Tris-HCl, pH 7.5, 75 mM KCl, 10 mM $MgCl_2$, 5 mM EDTA (TKME Buffer) and 4 μM $Hsp90_{Ec}$ and 4 μM CbpA cysteine mutants as indicated. Proteins were crosslinked in the presence of 0.8 mM DTME at 23 °C for 1 hr and analyzed by Coomassie staining following SDS-PAGE. Crosslinked species were excised and treated with NuPAGE LDS Sample Buffer (Invitrogen NP0007) containing DTT (50 mM) and re-analyzed by Coomassie staining following SDS-PAGE.

Crosslinking and mass spectrometry

DSSO or TMEA crosslinking was carried out as described above. Samples from DSSO crosslinking assays were analyzed using 3–8% Tris-acetate gels (Invitrogen EA03752BOX). Specific crosslinked protein bands were in-gel digested with trypsin for 16 h at 37 °C, as described [51]. The extracted peptides were dried and lyophilized prior to mass spectrometry analysis. Each sample was separated on a 75 μm × 15 cm, 2 μm Acclaim PepMap reverse phase column (Thermo) using an UltiMate 3000 RSLCnano HPLC (Thermo) at a flow rate of 300 nL/min followed by online analysis by tandem mass spectrometry using a Thermo Orbitrap Fusion mass spectrometer. For analysis of TMEA crosslinked proteins, peptides were eluted into the mass spectrometer using a 30 min gradient and parent full-scan mass spectra were collected in the Orbitrap mass analyzer at 120,000 FWHM resolution followed by HCD fragmentation (HCD normalized energy 32%, stepped ± 3%), and MS2 spectra collected in the ion trap. For analysis of DSSO crosslinked proteins, peptides were eluted into the mass spectrometer using a 120 min gradient. Parent full-scan mass spectra were collected in the Orbitrap at 120,000 FWHM resolution followed by CID fragmentation and collection of MS2 spectra in the Orbritrap at 30,000 FWHM resolution. Upon detection of fragment pairs with a mass difference of 31.9721 Da, consistent with cleavage of the DSSO crosslinker, each fragment of the pair was separately isolated, fragmented with HCD and an MS3 scan collected in the ion trap.

The mass spectrometry data were analyzed in Proteome Discoverer 2.4 (Thermo). Proteins were searched against *E. coli* proteins from the UniProt database using SequestHT. The search was limited to tryptic peptides, with maximally two missed cleavages allowed. Cysteine carbamidomethylation was set as a fixed modification, and methionine oxidation set as a variable modification. The precursor mass tolerance was 10 ppm, and the fragment mass tolerance was 0.6 Da. Identification of DSSO crosslinked peptides was performed using the XLinkx node with the following settings: precursor mass tolerance: 10 p.p.m.; MS2 Orbitrap fragment mass tolerance: 20 p.p.m.; MS3 ion trap ion mass tolerance: 0.5 Da; static modification: cysteine carbamidomethylation; dynamic modification: methionine oxidation; maximum missed cleavages: 2. The Percolator node was used to score and rank peptide matches using a 1% false discovery rate. Spectra of crosslinked peptides were manually inspected.

Western Blotting

Following TMEA crosslinking and SDS-PAGE, proteins were transferred to nitrocellulose membranes, stained with Ponceau S followed by immunodetection using rabbit CbpA antiserum. Membranes were imaged on a ChemiDoc MP imager.

Pull-down assay

DnaJ, CbpA and Ydj1 were biotin labeled as previously described [27]. DnaK D45C was biotin labeled as previously described [10]. Biotin-labeled DnaJ or CbpA (2 μM) was incubated for 5 min at 23 °C in reaction mixtures (50 μL) containing 20 mM Tris-HCl, pH 7.5, 75 mM KCl, 10 mM $MgCl_2$, 0.01% Triton X-100 (vol/vol) with $Hsp90_{Ec}$ wild-type or mutant, L2, and ATP as indicated. For DnaK D45C-biotin pull-down of $Hsp90_{Ec}$, 2 μM biotin-labeled DnaK D45C, 2 μM L2, and 6 μM $Hsp90_{Ec}$ were used with 0.03% Triton X-100 (vol/vol) in the reaction buffer. For $Hsp90_{Ec}$ MD and NTD pull-downs with L2 present, 2 μM biotin-labeled CbpA, 2 μM L2, and 4 μM $Hsp90_{Ec}$ were used with 0.05% Triton X-100 (vol/vol) in the reaction buffer. $Hsp90_{Ec}$ CTD pull-downs with L2 present were performed as described for the $Hsp90_{Ec}$ MD and NTD pull-downs, but with 0.01% Triton X-100 instead. Biotin-labeled Ydj1 (1.8 μM) was incubated for 5 min at 23 °C in 50 μL reaction mixtures containing 20 mM Tris-HCl, pH 7.5, 25 mM KCl, 5% glycerol (vol/vol), 0.01% Triton X-100 (vol/vol), 2 mM DTT, 10 mM $MgCl_2$ with Hsp82 wild-type or mutant, L2, and ATP as indicated. Streptavidin beads (20 μL 1:1 slurry) (Thermo, Invitrogen 65602) were then added and incubated 5 min at 25 °C with mixing for *E. coli* proteins or incubated 5 min at 30 °C with mixing for yeast proteins. The reaction mixtures were subject to magnetic separation for 2 min and washed twice with 0.4 mL of reaction buffer. Bound proteins were eluted with NuPAGE LDS Sample Buffer (Invitrogen NP0007) and heated at 85 °C for 5 min. DTT (50 mM) was added and the samples were analyzed by SDS-PAGE followed by Coomassie blue staining. Protein band intensities from replicate gels were quantified using ImageJ (http://imagej.nih.gov/ij) or BioRad Image Lab version 6.1.0. Any non-specific protein binding observed with the streptavidin beads alone was subtracted and for each lane the biotinylated protein was used for normalization. Statistical analysis was carried out in Prism 9 for Mac (GraphPad Software version 9.4.1) using one-way Anova followed by Dunnett's multiple comparisons analysis or two-way ANOVA followed by Bonferroni's multiple comparisons analysis.

BioLayer Interferometry (BLI)

BLI was used to monitor the interaction between *E. coli* and yeast Hsp90 and Hsp40 proteins using a Sartorius Octet N1 instrument and streptavidin biosensors at 23 °C. Ydj1-biotin (0.18 μM) was loaded on the biosensors and then the sensors were blocked with 10 μg/mL biocytin (Sigma B4261). The association of Hsp82 (1.4 – 22 μM) with Ydj1 was monitored over time followed by dissociation in the absence of Hsp82. All Ydj1, Hsp82 BLI steps were performed in 20 mM Tris pH 7.5, 50 mM KCl, 10 mM $MgCl_2$, 0.01% Triton X-100 (vol/vol), 0.02% Tween-20 (vol/vol) and 1 mg/mL BSA. The interaction of CbpA-biotin (0.23 μM) and DnaJ-biotin (0.15 μM) with $Hsp90_{Ec}$ (2.3 – 144 μM) was measured in 25 mM sodium phosphate pH 7.5, 50 mM KCl and 0.02 % Tween-20 (vol/vol) as described above for Ydj1 and Hsp82. For each experiment, nonspecific binding was monitored using a reference biosensor subjected to each of the above steps in the absence of the biotinylated protein, and the nonspecific binding signal was subtracted from the corresponding experiment. For steady-state analysis of kinetic association data, the association phase from three replicates at each Hsp90 concentration was fit using a single exponential equation in Prism 9 for Mac (GraphPad Software version 9.4.1), and the plateau value determined from the fit was plotted versus the concentration of Hsp90. The resulting

binding curve was analyzed using a one-site specific binding model in Prism to determine the K_d (equilibrium binding constant) and B_{max} (maximum specific binding) values.

GFP reactivation

GFP reactivation was performed as previously described [27]. Heat denatured GFP was added to reactions (100 μl) containing 25 mM Hepes, pH 7.5, 50 mM KCl, 0.1 mM EDTA, 2 mM DTT, 10 mM $MgCl_2$, 50 μg/ml bovine serum albumin (BSA), 4 mM ATP, an ATP regenerating system (10 mM creatine phosphate, 3 μg creatine kinase), 2 μM DnaK, 1 μM CbpA and 0.5 μM $Hsp90_{Ec}$ wild-type or mutant. Reactivation was monitored over time at 25 °C using a Tecan Infinite M200Pro plate reader. Excitation and emission wavelengths were 395 nm and 510 nm, respectively.

Luciferase reactivation

Luciferase (8 μM) was chemically denatured in 5M guanidine hydrochloride, 25 mM Hepes pH 7.5, 50 mM KCl, 0.1mM EDTA, 4 mM DTT for 10 min at 23 °C. For reactivation, denatured luciferase was diluted 100-fold into 25 mM Hepes pH 7.5, 0.1 M KOAc, 5 mM DTT, 10 mM $Mg(OAc)_2$, 100 μg/ml BSA, 2 mM ATP, an ATP regenerating system (10 mM creatine phosphate, 3 μg creatine kinase), 2 μM DnaK, 0.3 μM CbpA wild-type or mutant, 0.05 μM GrpE and 0.5 μM $Hsp90_{Ec}$ wild-type or mutant. Aliquots were removed at the indicated times and light output was measured using a Tecan Infinite M200Pro in luminescence mode with an integration time of 1000 ms following the injection of luciferin (50 μg/ml). Reactivation was determined compared to a non-denatured luciferase control. To test the activity of CbpA mutants in the absence of $Hsp90_{Ec}$, luciferase reactivation was carried our as described above using 1 μM DnaK, 0.1 μM CbpA wild-type or mutant and 0.05 μM GrpE.

ATPase activity

Steady-state ATP hydrolysis was measured at 37 °C in 20 mM Tris pH 7.5, 50 mM KCl, 2 mM DTT, 0.005 % (vol/vol) Triton X-100, 5 mM $MgCl_2$, and 2 mM ATP using a pyruvate kinase/lactate dehydrogenase enzyme-coupled assay as described [18] and 1 μM $Hsp90_{Ec}$ wild-type or mutant, 1.5 μM ribosomal L2 and 30 μg/ml geldanamycin as indicated. For $Hsp90_{Ec}$ CTD ATPase assays, 2 μM ribosomal L2 was used.

Molecular docking

Structure preparation—The crystal structure of apo $Hsp90_{Ec}$ was obtained from the protein databank as PDB ID 2IOQ [39]. The crystal structure of DnaK was obtained for the ADP configuration (PDB ID 2KHO [38]) and the NBD was used (residues 1–390). The crystal structure of the CbpA J-domain (residues 1–72) was obtained from PDB ID 2KQX [40]. The structures were prepared with the CHARMM36 force field using CHARMM-GUI [52–54] and any missing atoms and residues were built. The dimeric $Hsp90_{Ec}$ structure was generated by aligning two prepared monomers with each protomer of the biological assembly of PDB ID 2IOQ in PyMOL [55]. Docking was carried out with a single protomer of $Hsp90_{Ec}$ and the dimeric structures were only used for visualization of the docking results.

Molecular docking—The structures of $Hsp90_{Ec}$, DnaK and CbpA were prepared for modeling as described above. Docking was carried out using HADDOCK 2.4–2022.08 [56, 57]. Binary complexes were generated using ambiguous restraints from defined regions important for the interaction, as determined experimentally (Table S1). Passive residues were defined as residues within 6.5 Å of active residues that also had at least 15% relative solvent accessibility. This method was validated for the $Hsp90_{Ec}$-DnaK complex and reproduced the docked model reported previously [12]. Ternary complexes were created using ambiguous restraints from defined regions in addition to unambiguous distance restraints informed by the crosslinking experiments (Table S1). Given the trifunctional cross-linker arm distance of 10.3 Å and application of the distance restraints at the alpha carbons, a slightly larger restraint distance of 12 Å was allowed. Center of mass restraints were implemented in docking for ternary complexes to ensure all molecules are in contact. The random removal of ambiguous interaction restraints option was selected for docking in both binary and ternary complexes.

Supplementary Material

Refer to Web version on PubMed Central for supplementary material.

Acknowledgements

We thank Susan Gottesman and Kumaran Ramamurthi for helpful discussions. We also thank the CCR Genomics Core, Center for Cancer Research, National Cancer Institute, National Institutes of Health. This research was supported by the Intramural Research Program of the NIH, NCI, Center for Cancer Research (SW) and the National Institute of General Medical Sciences of the National Institutes of Health under Award Number R35GM146963 (ANK).

Abbreviations:

$Hsp90_{Ec}$	*E. coli* Hsp90
Hsp90 NTD	Hsp90 N-terminal domain
Hsp90 MD	Hsp90 middle domain
Hsp90 CTD	Hsp90 C-terminal domain
Hsp70 NBD	Hsp70 nucleotide binding domain
Hsp70 SDB	Hsp70 substrate binding domain
JDP	J-domain protein

References

[1]. Mayer MP, Gierasch LM. Recent advances in the structural and mechanistic aspects of Hsp70 molecular chaperones. J Biol Chem. 2019;294:2085–97. [PubMed: 30455352]

[2]. Rosenzweig R, Nillegoda NB, Mayer MP, Bukau B. The Hsp70 chaperone network. Nat Rev Mol Cell Biol. 2019;20:665–80. [PubMed: 31253954]

[3]. Schopf FH, Biebl MM, Buchner J. The HSP90 chaperone machinery. Nat Rev Mol Cell Biol. 2017;18:345–60. [PubMed: 28429788]

[4]. Wickner S, Nguyen TL, Genest O. The Bacterial Hsp90 Chaperone: Cellular Functions and Mechanism of Action. Annu Rev Microbiol. 2021;75:719–39. [PubMed: 34375543]

[5]. Bardwell JC, Craig EA. Ancient heat shock gene is dispensable. J Bacteriol. 1988;170:2977–83. [PubMed: 3290192]

[6]. Lindquist S The heat-shock response. Annu Rev Biochem. 1986;55:1151–91. [PubMed: 2427013]

[7]. Honore FA, Mejean V, Genest O. Hsp90 Is Essential under Heat Stress in the Bacterium Shewanella oneidensis. Cell Rep. 2017;19:680–7. [PubMed: 28445720]

[8]. Biebl MM, Buchner J. Structure, Function, and Regulation of the Hsp90 Machinery. Cold Spring Harb Perspect Biol. 2019;11.

[9]. Genest O, Hoskins JR, Camberg JL, Doyle SM, Wickner S. Heat shock protein 90 from Escherichia coli collaborates with the DnaK chaperone system in client protein remodeling. Proc Natl Acad Sci U S A. 2011;108:8206–11. [PubMed: 21525416]

[10]. Genest O, Hoskins JR, Kravats AN, Doyle SM, Wickner S. Hsp70 and Hsp90 of E. coli Directly Interact for Collaboration in Protein Remodeling. J Mol Biol. 2015;427:3877–89. [PubMed: 26482100]

[11]. Kirschke E, Goswami D, Southworth D, Griffin PR, Agard DA. Glucocorticoid receptor function regulated by coordinated action of the Hsp90 and Hsp70 chaperone cycles. Cell. 2014;157:1685–97. [PubMed: 24949977]

[12]. Kravats AN, Doyle SM, Hoskins JR, Genest O, Doody E, Wickner S. Interaction of E. coli Hsp90 with DnaK Involves the DnaJ Binding Region of DnaK. J Mol Biol. 2017;429:858–72. [PubMed: 28013030]

[13]. Kravats AN, Hoskins JR, Reidy M, Johnson JL, Doyle SM, Genest O, et al. Functional and physical interaction between yeast Hsp90 and Hsp70. Proc Natl Acad Sci U S A. 2018;115:E2210–E9. [PubMed: 29463764]

[14]. Moran Luengo T, Kityk R, Mayer MP, Rudiger SGD. Hsp90 Breaks the Deadlock of the Hsp70 Chaperone System. Mol Cell. 2018;70:545–52 e9. [PubMed: 29706537]

[15]. Johnson JL. Evolution and function of diverse Hsp90 homologs and cochaperone proteins. Biochim Biophys Acta. 2012;1823:607–13. [PubMed: 22008467]

[16]. Mayer MP, Le Breton L. Hsp90: breaking the symmetry. Mol Cell. 2015;58:8–20. [PubMed: 25839432]

[17]. Rohl A, Rohrberg J, Buchner J. The chaperone Hsp90: changing partners for demanding clients. Trends Biochem Sci. 2013;38:253–62. [PubMed: 23507089]

[18]. Graf C, Stankiewicz M, Kramer G, Mayer MP. Spatially and kinetically resolved changes in the conformational dynamics of the Hsp90 chaperone machine. EMBO J. 2009;28:602–13. [PubMed: 19165152]

[19]. Hessling M, Richter K, Buchner J. Dissection of the ATP-induced conformational cycle of the molecular chaperone Hsp90. Nat Struct Mol Biol. 2009;16:287–93. [PubMed: 19234467]

[20]. Taipale M, Jarosz DF, Lindquist S. HSP90 at the hub of protein homeostasis: emerging mechanistic insights. Nat Rev Mol Cell Biol. 2010;11:515–28. [PubMed: 20531426]

[21]. Zuehlke A, Johnson JL. Hsp90 and co-chaperones twist the functions of diverse client proteins. Biopolymers. 2010;93:211–7. [PubMed: 19697319]

[22]. Dean ME, Johnson JL. Human Hsp90 cochaperones: perspectives on tissue-specific expression and identification of cochaperones with similar in vivo functions. Cell Stress Chaperones. 2021;26:3–13. [PubMed: 33037995]

[23]. Kampinga HH, Craig EA. The HSP70 chaperone machinery: J proteins as drivers of functional specificity. Nat Rev Mol Cell Biol. 2010;11:579–92. [PubMed: 20651708]

[24]. Craig EA, Marszalek J. How Do J-Proteins Get Hsp70 to Do So Many Different Things? Trends Biochem Sci. 2017;42:355–68. [PubMed: 28314505]

[25]. Bracher A, Verghese J. The nucleotide exchange factors of Hsp70 molecular chaperones. Front Mol Biosci. 2015;2:10. [PubMed: 26913285]

[26]. Genest O, Wickner S, Doyle SM. Hsp90 and Hsp70 chaperones: Collaborators in protein remodeling. J Biol Chem. 2019;294:2109–20. [PubMed: 30401745]

[27]. Doyle SM, Hoskins JR, Kravats AN, Heffner AL, Garikapati S, Wickner S. Intermolecular Interactions between Hsp90 and Hsp70. J Mol Biol. 2019;431:2729–46. [PubMed: 31125567]

[28]. Sun M, Kotler JLM, Liu S, Street TO. The endoplasmic reticulum (ER) chaperones BiP and Grp94 selectively associate when BiP is in the ADP conformation. J Biol Chem. 2019;294:6387–96. [PubMed: 30787103]

[29]. Gassler CS, Buchberger A, Laufen T, Mayer MP, Schroder H, Valencia A, et al. Mutations in the DnaK chaperone affecting interaction with the DnaJ cochaperone. Proc Natl Acad Sci U S A. 1998;95:15229–34. [PubMed: 9860951]

[30]. Suh WC, Burkholder WF, Lu CZ, Zhao X, Gottesman ME, Gross CA. Interaction of the Hsp70 molecular chaperone, DnaK, with its cochaperone DnaJ. Proc Natl Acad Sci U S A. 1998;95:15223–8. [PubMed: 9860950]

[31]. Ahmad A, Bhattacharya A, McDonald RA, Cordes M, Ellington B, Bertelsen EB, et al. Heat shock protein 70 kDa chaperone/DnaJ cochaperone complex employs an unusual dynamic interface. Proc Natl Acad Sci U S A. 2011;108:18966–71. [PubMed: 22065753]

[32]. Kityk R, Kopp J, Mayer MP. Molecular Mechanism of J-Domain-Triggered ATP Hydrolysis by Hsp70 Chaperones. Mol Cell. 2018;69:227–37 e4. [PubMed: 29290615]

[33]. Obermann WM, Sondermann H, Russo AA, Pavletich NP, Hartl FU. In vivo function of Hsp90 is dependent on ATP binding and ATP hydrolysis. J Cell Biol. 1998;143:901–10. [PubMed: 9817749]

[34]. Panaretou B, Prodromou C, Roe SM, O'Brien R, Ladbury JE, Piper PW, et al. ATP binding and hydrolysis are essential to the function of the Hsp90 molecular chaperone in vivo. EMBO J. 1998;17:4829–36. [PubMed: 9707442]

[35]. Barthel TK, Zhang J, Walker GC. ATPase-defective derivatives of Escherichia coli DnaK that behave differently with respect to ATP-induced conformational change and peptide release. J Bacteriol. 2001;183:5482–90. [PubMed: 11544208]

[36]. Bird JG, Sharma S, Roshwalb SC, Hoskins JR, Wickner S. Functional analysis of CbpA, a DnaJ homolog and nucleoid-associated DNA-binding protein. J Biol Chem. 2006;281:34349–56. [PubMed: 16973605]

[37]. Nakamoto H, Fujita K, Ohtaki A, Watanabe S, Narumi S, Maruyama T, et al. Physical interaction between bacterial heat shock protein (Hsp) 90 and Hsp70 chaperones mediates their cooperative action to refold denatured proteins. J Biol Chem. 2014;289:6110–9. [PubMed: 24415765]

[38]. Bertelsen EB, Chang L, Gestwicki JE, Zuiderweg ER. Solution conformation of wild-type E. coli Hsp70 (DnaK) chaperone complexed with ADP and substrate. Proc Natl Acad Sci U S A. 2009;106:8471–6. [PubMed: 19439666]

[39]. Shiau AK, Harris SF, Southworth DR, Agard DA. Structural Analysis of E. coli hsp90 reveals dramatic nucleotide-dependent conformational rearrangements. Cell. 2006;127:329–40. [PubMed: 17055434]

[40]. Sarraf NS, Baardsnes J, Cheng J, O'Connor-McCourt M, Cygler M, Ekiel I. Structural basis of the regulation of the CbpA co-chaperone by its specific modulator CbpM. J Mol Biol. 2010;398:111–21. [PubMed: 20226195]

[41]. Noddings CM, Wang RY, Johnson JL, Agard DA. Structure of Hsp90-p23-GR reveals the Hsp90 client-remodelling mechanism. Nature. 2022;601:465–9. [PubMed: 34937936]

[42]. Wang RY, Noddings CM, Kirschke E, Myasnikov AG, Johnson JL, Agard DA. Structure of Hsp90-Hsp70-Hop-GR reveals the Hsp90 client-loading mechanism. Nature. 2022;601:460–4. [PubMed: 34937942]

[43]. Biebl MM, Delhommel F, Faust O, Zak KM, Agam G, Guo X, et al. NudC guides client transfer between the Hsp40/70 and Hsp90 chaperone systems. Mol Cell. 2022;82:555–69 e7. [PubMed: 35063133]

[44]. Backe SJ, Sager RA, Woodford MR, Makedon AM, Mollapour M. Post-translational modifications of Hsp90 and translating the chaperone code.

[45]. Skowyra D, Wickner S. The interplay of the GrpE heat shock protein and Mg2+ in RepA monomerization by DnaJ and DnaK. J Biol Chem. 1993;268:25296–301. [PubMed: 8244960]

[46]. Ueguchi C, Kakeda M, Yamada H, Mizuno T. An analogue of the DnaJ molecular chaperone in Escherichia coli. Proc Natl Acad Sci U S A. 1994;91:1054–8. [PubMed: 8302830]

[47]. Genest O, Reidy M, Street TO, Hoskins JR, Camberg JL, Agard DA, et al. Uncovering a region of heat shock protein 90 important for client binding in E. coli and chaperone function in yeast. Mol Cell. 2013;49:464–73. [PubMed: 23260660]

[48]. Miot M, Reidy M, Doyle SM, Hoskins JR, Johnston DM, Genest O, et al. Species-specific collaboration of heat shock proteins (Hsp) 70 and 100 in thermotolerance and protein disaggregation. Proc Natl Acad Sci U S A. 2011;108:6915–20. [PubMed: 21474779]

[49]. Reidy M, Sharma R, Roberts BL, Masison DC. Human J-protein DnaJB6b Cures a Subset of Saccharomyces cerevisiae Prions and Selectively Blocks Assembly of Structurally Related Amyloids. J Biol Chem. 2016;291:4035–47. [PubMed: 26702057]

[50]. Motojima-Miyazaki Y, Yoshida M, Motojima F. Ribosomal protein L2 associates with E. coli HtpG and activates its ATPase activity. Biochem Biophys Res Commun. 2010;400:241–5. [PubMed: 20727857]

[51]. Shevchenko A, Tomas H, Havlis J, Olsen JV, Mann M. In-gel digestion for mass spectrometric characterization of proteins and proteomes. Nat Protoc. 2006;1:2856–60. [PubMed: 17406544]

[52]. Jo S, Kim T, Iyer VG, Im W. CHARMM-GUI: a web-based graphical user interface for CHARMM. J Comput Chem. 2008;29:1859–65. [PubMed: 18351591]

[53]. Jo S, Cheng X, Islam SM, Huang L, Rui H, Zhu A, et al. CHARMM-GUI PDB manipulator for advanced modeling and simulations of proteins containing nonstandard residues. Adv Protein Chem Struct Biol. 2014;96:235–65. [PubMed: 25443960]

[54]. Park S-J, Kern N, Brown T, Lee J, Im W. CHARMM-GUI PDB Manipulator: Various PDB Structural Modifications for Biomolecular Modeling and Simulation. Journal of Molecular Biology. 2023:167995. [PubMed: 37356910]

[55]. PyMOL. The PyMOL Molecular Graphics System, Version 2.0 Schrödinger, LLC.

[56]. van Zundert GCP, Rodrigues J, Trellet M, Schmitz C, Kastritis PL, Karaca E, et al. The HADDOCK2.2 Web Server: User-Friendly Integrative Modeling of Biomolecular Complexes. J Mol Biol. 2016;428:720–5. [PubMed: 26410586]

[57]. Honorato RV, Koukos PI, Jimenez-Garcia B, Tsaregorodtsev A, Verlato M, Giachetti A, et al. Structural Biology in the Clouds: The WeNMR-EOSC Ecosystem. Front Mol Biosci. 2021;8:729513. [PubMed: 34395534]

Highlights

- *E. coli* Hsp90, Hsp70 and J-domain protein collaborate in protein remodeling
- *E. coli* Hsp90, Hsp70 (DnaK) and J-domain protein (CbpA) interact directly
- Hsp90's middle domain contacts the DnaK J-domain binding site and the CbpA J-domain
- The J-domain of CbpA is sufficient for complex formation with Hsp90 and Hsp70
- *E. coli* and yeast Hsp90s form binary complexes with J-domain proteins

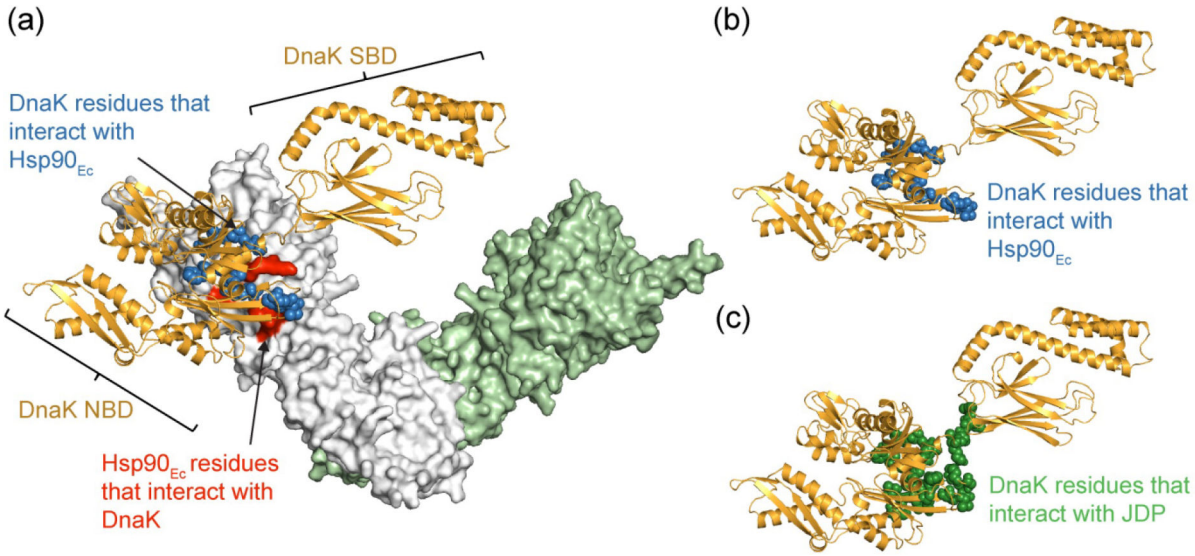

Figure 1. Models depicting overlapping sites of $Hsp90_{Ec}$ and JDP interaction on DnaK.

(a) Docked model of apo $Hsp90_{Ec}$ dimer (green and grey surface model) in complex with ADP-bound conformation of DnaK (gold cartoon) [12]. $Hsp90_{Ec}$ residues that interact with DnaK are shown in red [10] and DnaK residues that interact with $Hsp90_{Ec}$ are shown in blue spheres [12]. (b) DnaK cartoon model (gold) depicting the DnaK residues that interact with $Hsp90_{Ec}$ (blue spheres) [12]. (c) DnaK cartoon model (gold) depicting the DnaK residues that interact with JDP (green spheres) [29–31].

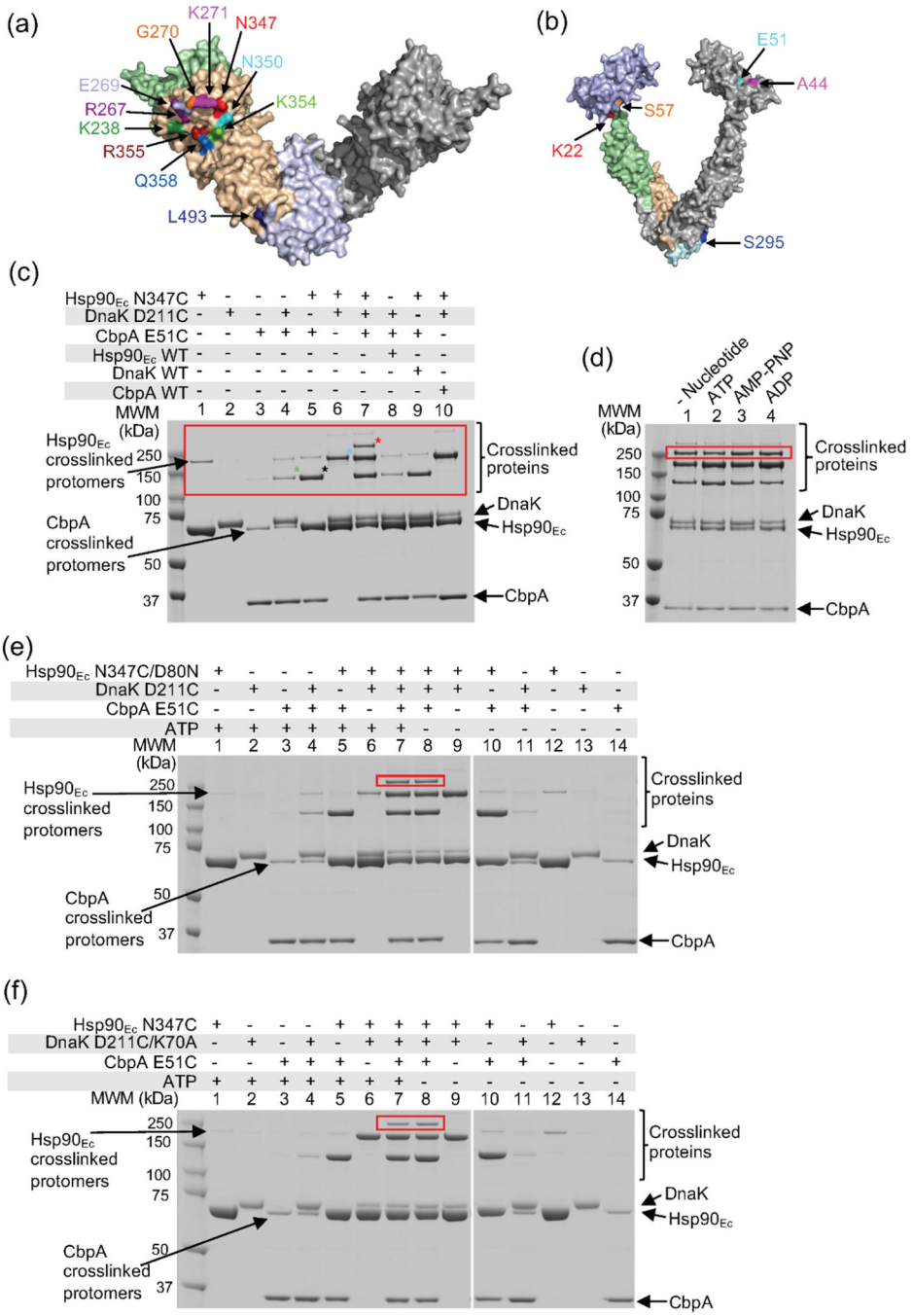

Figure 2. Formation of a novel ternary complex.

(a) AlphaFold model of $Hsp90_{Ec}$ dimer in the apo form showing residues in the MD discussed in this paper. One protomer is gray and the other is colored as follows: NTD is green, the MD is tan and the CTD is lavender. (b) AlphaFold model of CbpA dimer showing residues discussed in this paper. One protomer is gray and the other is colored as follows: J-domain is lavender, CTD I is green, CTD II is tan, and the dimerization domain is light blue. Modeling details for $Hsp90_{Ec}$ and CbpA can be found in Materials and Methods. (c) Crosslinking between $Hsp90_{Ec}$ N347C, CbpA E51C, and DnaK D211C in

the presence of ATP. Cysteine mutant proteins were incubated with TMEA individually, in pairs and all three together as indicated and as described in Materials and Methods. In lanes 8–10, each cysteine mutant was substituted with the respective WT protein as indicated. Red, green, black and cyan asterisks indicate position of the potential $Hsp90_{Ec}$-DnaK-CbpA complex, DnaK-CbpA complex, $Hsp90_{Ec}$-CbpA complex, and $Hsp90_{Ec}$-DnaK complex, respectively. The red box indicates slowly migrating crosslinked products. A representative gel is shown, n=3. (d) TMEA crosslinking between $Hsp90_{Ec}$ N347C, CbpA E51C, and DnaK D211C with no nucleotide or with ATP, AMP-PNP or ADP present. (e) TMEA crosslinking between $Hsp90_{Ec}$ N347C/D80N, CbpA E51C, and DnaK D211C with and without ATP in the crosslinking reaction. (f) TMEA crosslinking, as described in Materials and Methods, between DnaK D211C/K70A, CbpA E51C, and $Hsp90_{Ec}$ N347C with and without ATP in the crosslinking reaction. In (d-f), a representative gel is shown (n=3) and the red box indicates the potential $Hsp90_{Ec}$-DnaK-CbpA complex.

(a)

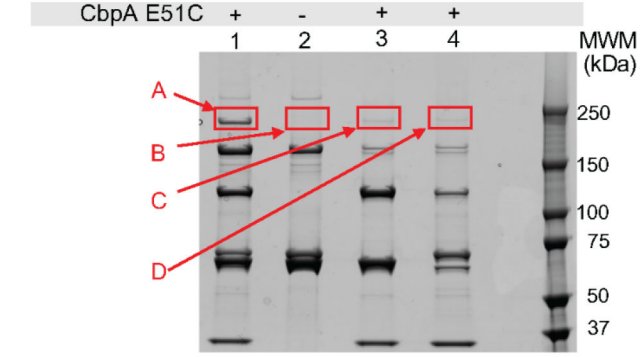

(b)

Sample	Protein identified	Coverage (%)	Peptides (#)	PSMs (#)
A	$Hsp90_{Ec}$	83	67	2659
	DnaK	80	70	1753
	CbpA	56	15	671
B	$Hsp90_{Ec}$	72	55	637
	DnaK	63	42	286
C	$Hsp90_{Ec}$	74	55	813
	CbpA	53	13	165
D	DnaK	66	50	416
	CbpA	44	12	131

Figure 3. The ternary complex is comprised of $Hsp90_{Ec}$, DnaK, and CbpA.

(a) 3–8% Tris-acetate gel of TMEA crosslinked products for mass spectrometry (MS) analysis. Red boxes indicate region of gel excised for MS analysis. (b) Mass spectrometry results indicating the protein composition of the species outlined in the red boxes from samples A-D in (a). PSMs, peptide spectral matches.

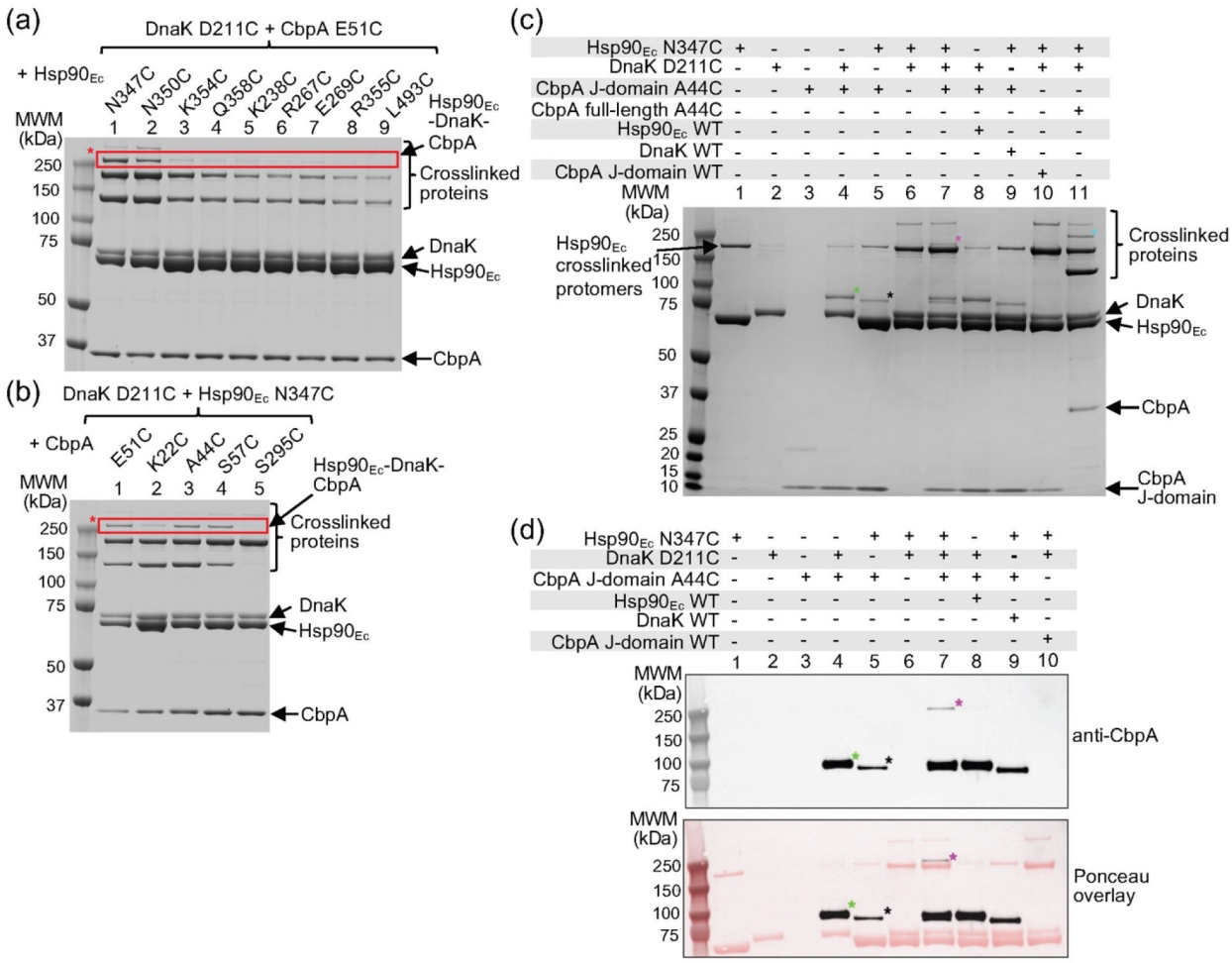

Figure 4. The sites of interaction in $Hsp90_{Ec}$, DnaK and CbpA involved in ternary complex formation.

(a) TMEA crosslinking with CbpA E51C, DnaK D211C, and $Hsp90_{Ec}$ MD mutants. L493C is an $Hsp90_{Ec}$ CTD mutant. (b) TMEA crosslinking with $Hsp90_{Ec}$ N347C, DnaK D211C and various CbpA mutants. CbpA S295C is a mutant in the dimerization domain. In (a-b) the red box indicates the expected position of the $Hsp90_{Ec}$-DnaK-CbpA complex and the asterisk points out the ternary complex. (c) TMEA crosslinking with CbpA A44C J-domain fragment, DnaK D211C, and $Hsp90_{Ec}$ N347C. Magenta, green, black, and cyan asterisks point out the $Hsp90_{Ec}$-DnaK-CbpA J-domain fragment complex, DnaK-CbpA J-domain complex, $Hsp90_{Ec}$-CbpA J-domain complex, and $Hsp90_{Ec}$-DnaK-CbpA full length complex, respectively. (d) TMEA crosslinking of CbpA J-domain fragment, DnaK, and $Hsp90_{Ec}$ followed by Western blot analysis using CbpA antiserum. Asterisks denote complexes mentioned in (c). Top panel is the CbpA immunoblot and bottom panel is CbpA immunoblot overlay with Ponceau S staining. In (a-d), TMEA crosslinking was carried out as described in Materials and Methods. Representitive gels of three replicates are shown.

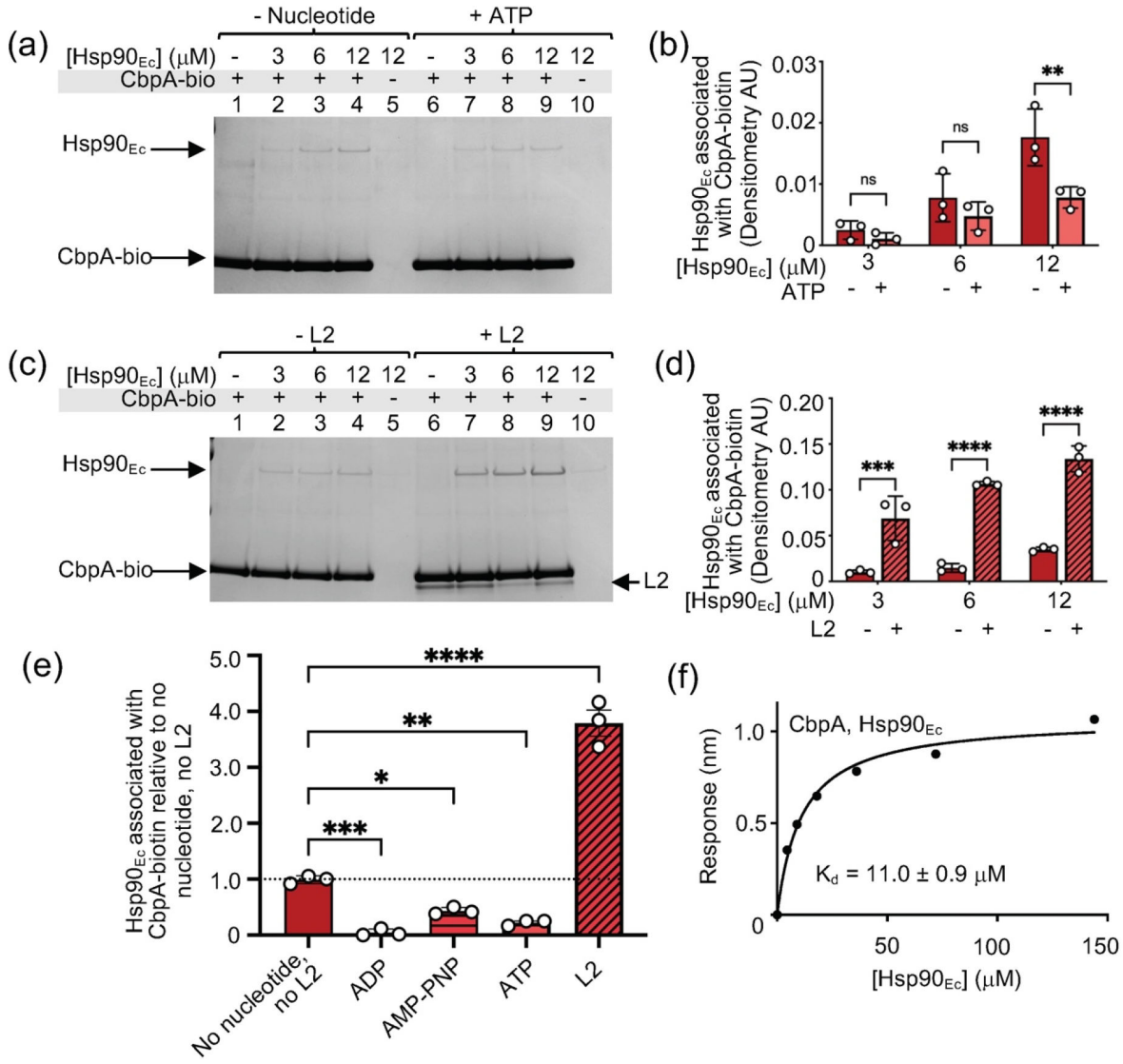

Figure 5. Interaction between $Hsp90_{Ec}$ and CbpA.

In vitro interaction between CbpA-biotin (2 μM) and $Hsp90_{Ec}$ (3–12 μM) in the presence and absence of (a) ATP (2 mM) or (c) L2 (2 μM) was monitored using a pull-down assay. The results were analyzed by SDS-PAGE followed by Coomassie blue staining. Densitometry analysis is shown in (b) and (d). In (b) and (d), results are shown as the means ± SD for three or more replicates. For statistical analysis, densitometry data from experiments with ATP or L2 were compared to data without ATP or L2 at each $Hsp90_{Ec}$ concentration using two-way Anova, n = 3, ** 0.001 < P < 0.01, *** 0.0001 < P < 0.001, ****P<0.0001. (e) Relative quantification of the $Hsp90_{Ec}$-CbpA interaction. Means ± SD are shown. The amount of $Hsp90_{Ec}$ that associated with CbpA when no nucleotide or client are present is compared to $Hsp90_{Ec}$-CbpA association when ADP, AMP-PNP, ATP, or L2 are present. The individual pull-downs and densitometry analysis when ADP and AMP-PNP are present are shown in Fig. S5. Statistical analysis was done using one-way Anova, n = 3, * 0.01 < P < 0.05, ** 0.001 < P < 0.01, *** 0.0001 < P < 0.001, ****P < 0.0001.

(f) $Hsp90_{Ec}$-CbpA interaction was assessed using BioLayer Interferometry as described in Materials and Methods.

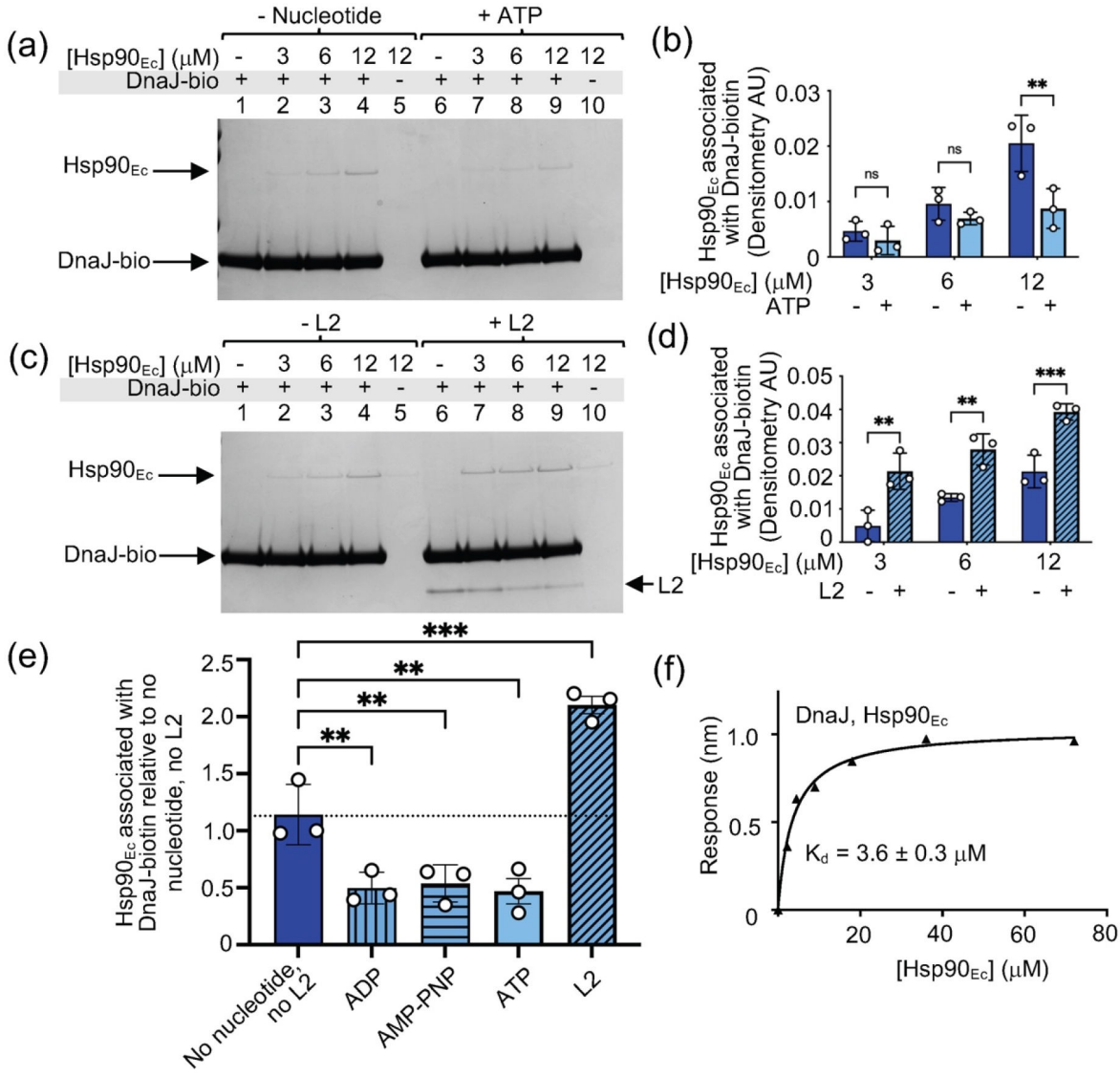

Figure 6. Interaction between Hsp90$_{Ec}$ and DnaJ.

In vitro interaction between DnaJ-biotin (2 μM) and Hsp90$_{Ec}$ (3–12 μM) in the presence and absence of (a) ATP (2 mM) or (c) L2 (2 μM) was monitored using a pull-down assay. The results were analyzed by SDS-PAGE followed by Coomassie blue staining. Densitometry analysis is shown in (b) and (d). In (b) and (d), results are shown as the means ± SD for three or more replicates. For statistical analysis, densitometry data from experiments with ATP or L2 were compared to data without ATP or L2 at each Hsp90$_{Ec}$ concentration using two-way Anova, n = 3, ** 0.001 < P < 0.01, *** 0.0001 < P < 0.001. (e) Relative quantification of the Hsp90$_{Ec}$-DnaJ interaction. Means ± SD are shown. The amount of Hsp90$_{Ec}$ that associated with DnaJ when no nucleotide or client are present is compared to Hsp90$_{Ec}$-DnaJ association when ADP, AMP-PNP, ATP, or L2 are present. The individual pull-downs and densitometry analysis when ADP and AMP-PNP are present are shown in Fig. S6. Statistical analysis was done using one-way Anova, n = 3, ** 0.001 < P <

0.01, *** 0.0001 < P < 0.001. (f) $Hsp90_{Ec}$-DnaJ interaction was assessed using BioLayer Interferometry as described in Materials and Methods.

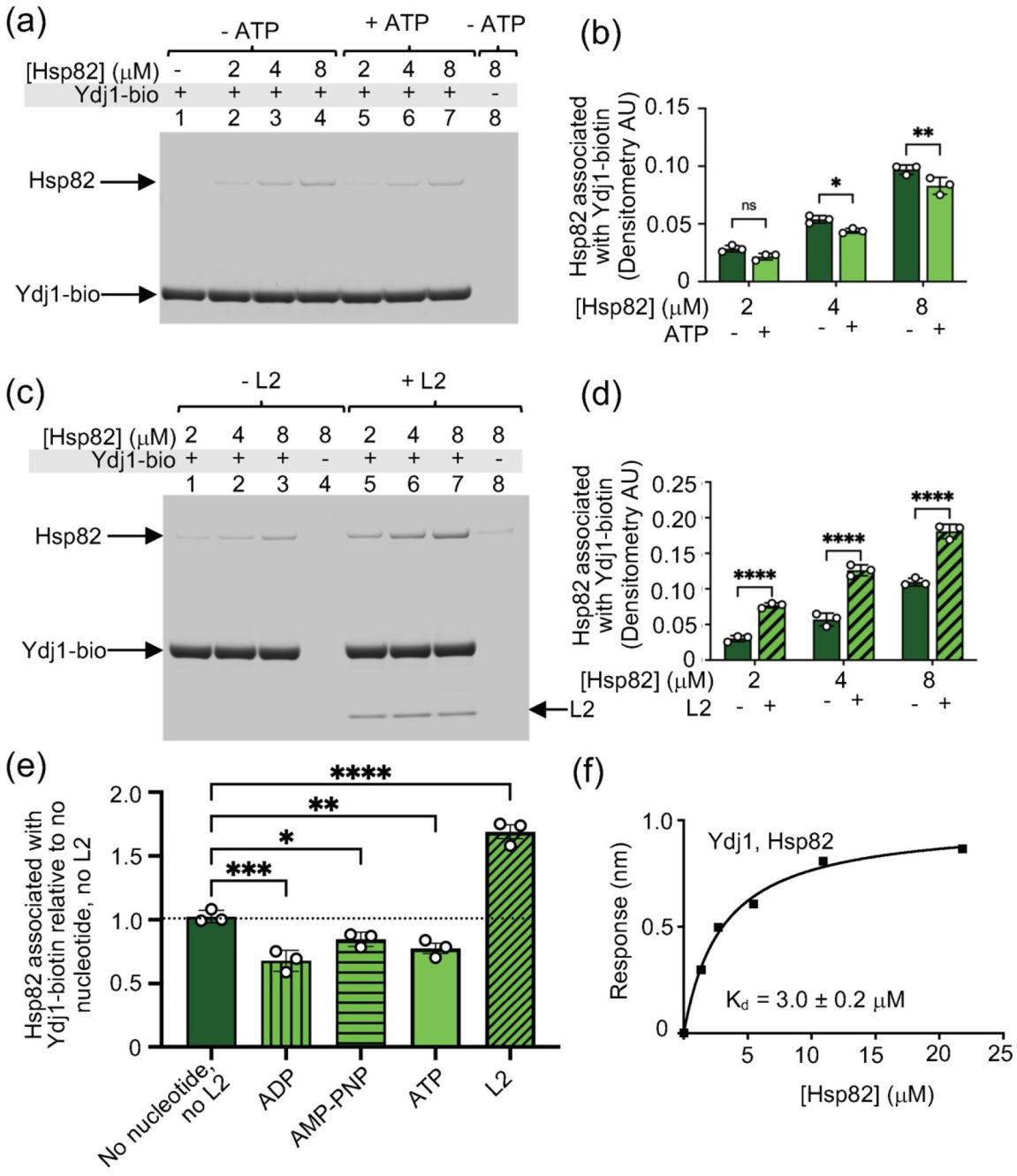

Figure 7. The Hsp90-J-domain protein interaction is conserved in yeast.

In vitro interaction between Ydj1-biotin (1.8 μM) and Hsp82 (2–8 μM) in the presence and absence of (a) ATP (2 mM) or (c) L2 (2 μM) was monitored using a pull-down assay. The results were analyzed by SDS-PAGE followed by Coomassie blue staining. For (a) and (c) a representative gel from three replicates is shown. Densitometry analysis is shown in (b) and (d) as means ± SD of three replicates. Pull-down assays and statistical analysis of densitometry data were performed as described in Fig. 4 and Fig. 5. * $0.01 < P < 0.05$, ** $0.001 < P < 0.01$, ****$P<0.0001$. (e) Relative quantification of the Hsp82-Ydj1 interaction. Means ± SD are shown. The amount of Hsp82 that associated with Ydj1 when no nucleotide

or client are present is compared to Hsp82-Ydj1 association when ADP, AMP-PNP, ATP, or L2 are present. The individual pull-downs and densitometry analysis when ADP and AMP-PNP are present are shown in Fig. S6. Statistical analysis was done using one-way Anova, n = 3, * $0.01 < P < 0.05$, ** $0.001 < P < 0.01$, *** $0.0001 < P < 0.001$, ****$P < 0.0001$. (f) BioLayer Interferometry was used to assess the K_d for the Hsp82-Ydj1 interaction as described in Materials and Methods.

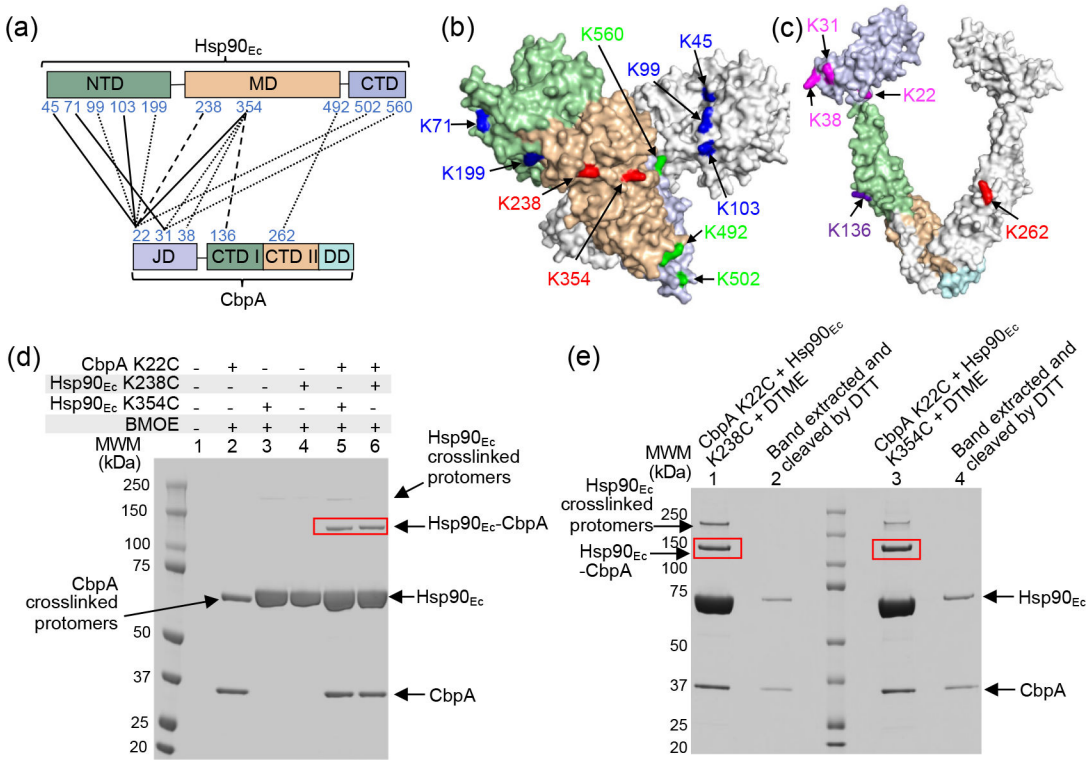

Figure 8. The sites of interaction between Hsp90$_{Ec}$ and CbpA.

(a) Schematic depicting sites of interaction between Hsp90$_{Ec}$ and CbpA identified by DSSO crosslinking followed by tandem mass spectrometry, n = 2. Identified intermolecular crosslinks are denoted using black lines with crosslinked lysine residues numbered in blue. Solid lines indicate crosslinks observed in both replicates, dashed lines indicate crosslinks seen twice in one replicate, and dotted lines indicate crosslinks observed once in either replicate. (b) Molecular model of an Hsp90$_{Ec}$ dimer showing positions of crosslinked residues identified in (a). One protomer is gray. In the other, the Hsp90$_{Ec}$ NTD is green, MD is tan and CTD is lavender. Hsp90$_{Ec}$ NTD residues are blue, MD residues are red and CTD residues are green. (c) Molecular model of a CbpA dimer showing positions of crosslinked residues identified in (a). One protomer is gray. In the other, the CbpA J-domain is lavender, CTD I is green, CTD II is tan and the dimerization domain is light blue. CbpA J-domain residues are magenta, the CTD I residue is purple and the CTD II residue is red. (d) BMOE crosslinking between CbpA and Hsp90$_{Ec}$ was carried out as described in Materials and Methods. Hsp90$_{Ec}$-CbpA crosslinked species are outlined with a red box. (e) DTME crosslinking of CbpA with Hsp90$_{Ec}$ MD mutants to assess the composition of the crosslinked species outlined by the red box in (d) was carried out as described in Materials and Methods. Crosslinked species were separated by SDS-PAGE, extracted and cleaved with DTT. The gel shows DTME crosslinked products before (lanes 1 and 3 (red boxes)), and after (lanes 2 and 4) extraction and cleavage with DTT. For (d-e), a representative of three replicates is shown.

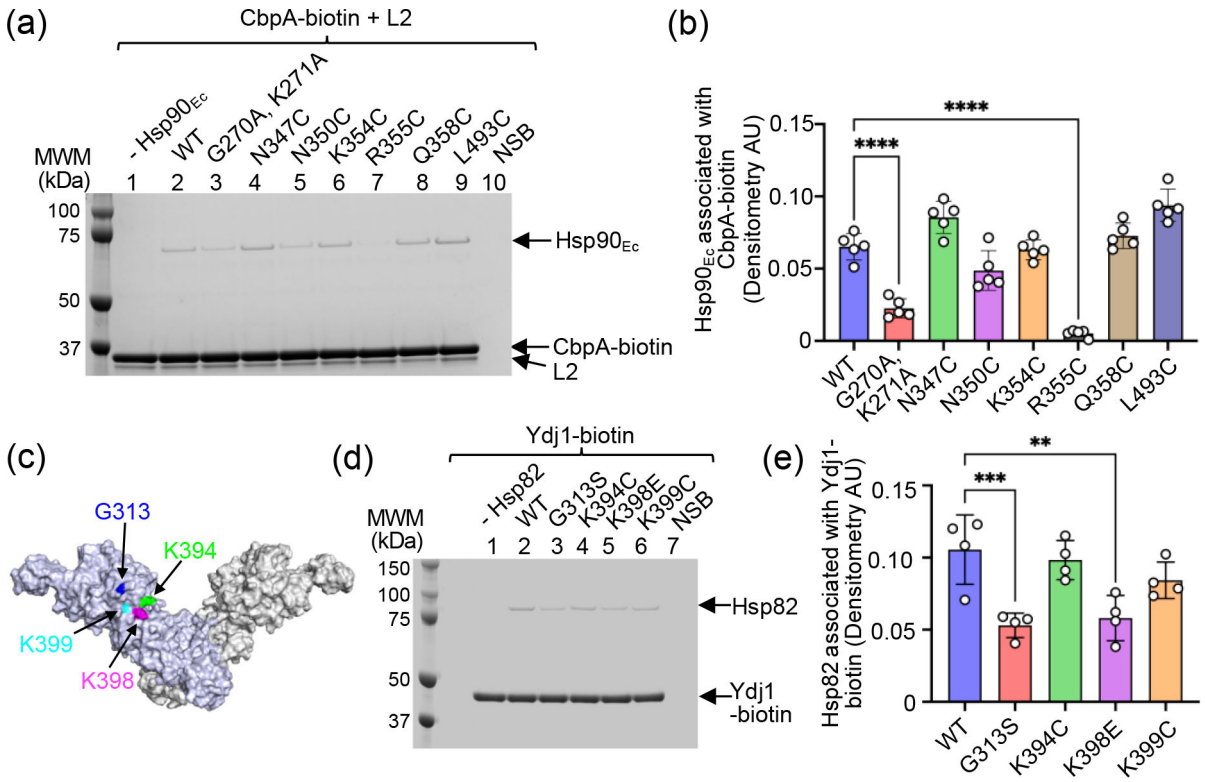

Figure 9. Interaction between J-domain protein and Hsp90 middle domain.

(a) The interaction between biotinylated CbpA and $Hsp90_{Ec}$ MD mutants in the presence of L2 was monitored using a pull-down assay. The results were analyzed by SDS-PAGE followed by Coomassie blue staining. (b) Quantification of $Hsp90_{Ec}$ associated with CbpA-biotin in the pull-downs shown in (a). Each $Hsp90_{Ec}$ MD mutant was compared to wild-type using one-way Anova, n = 5, ****P < 0.0001. (c) Molecular model of Hsp82 dimer showing locations of residues discussed in (d, e). One protomer is in lavender and the other is in gray. (d) The interaction between biotinylated Ydj1 and Hsp82 MD mutants was monitored using a pull-down assay. The results were analyzed by SDS-PAGE followed by Coomassie blue staining. (e) Quantification of Hsp82 associated with Ydj1-biotin in pull-downs shown in (d). Each $Hsp90_{Ec}$ MD mutant was compared to wild-type using one-way Anova, n = 4, ** 0.001 < P < 0.01, *** 0.0001 < P < 0.001. Pull-down assays were carried out as described in Materials and Methods and a representative gel of four or more replicates are shown in (a) and (d). In (b) and (e) results are shown as means ± SD.

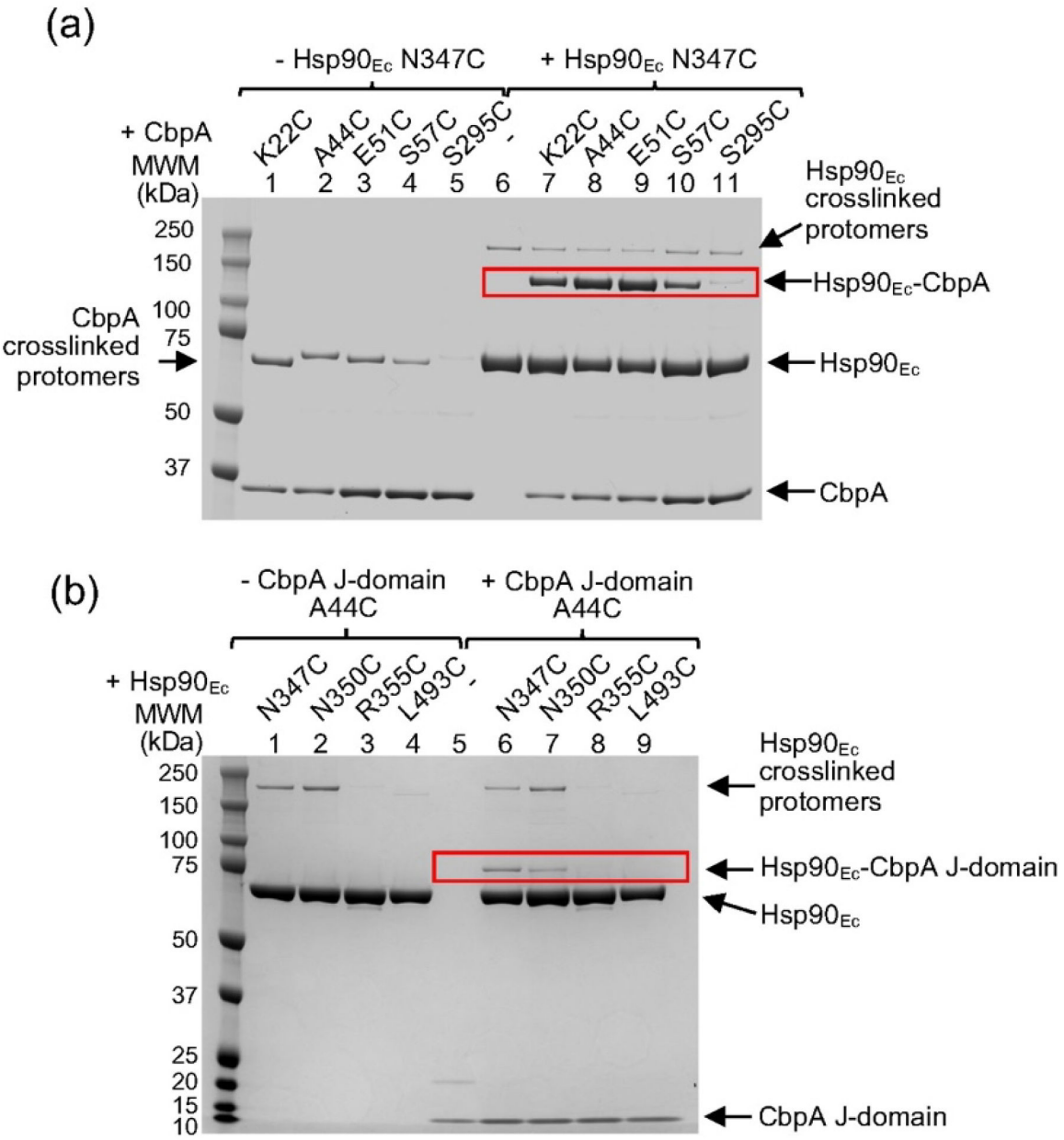

Figure 10. The role of the CbpA J-domain in CbpA-Hsp90$_{Ec}$ complex formation.

(a) BMOE crosslinking between Hsp90$_{Ec}$ N347C and CbpA J-domain mutants. CbpA S295C is a mutant in the dimerization domain. (b) BMOE crosslinking with CbpA A44C J-domain fragment and Hsp90$_{Ec}$ N347C, N350C, R355C, or L493C. Red boxes indicate Hsp90$_{Ec}$-CbpA or Hsp90$_{Ec}$-CbpA J-domain complexes. Representative gels are shown (n=3).

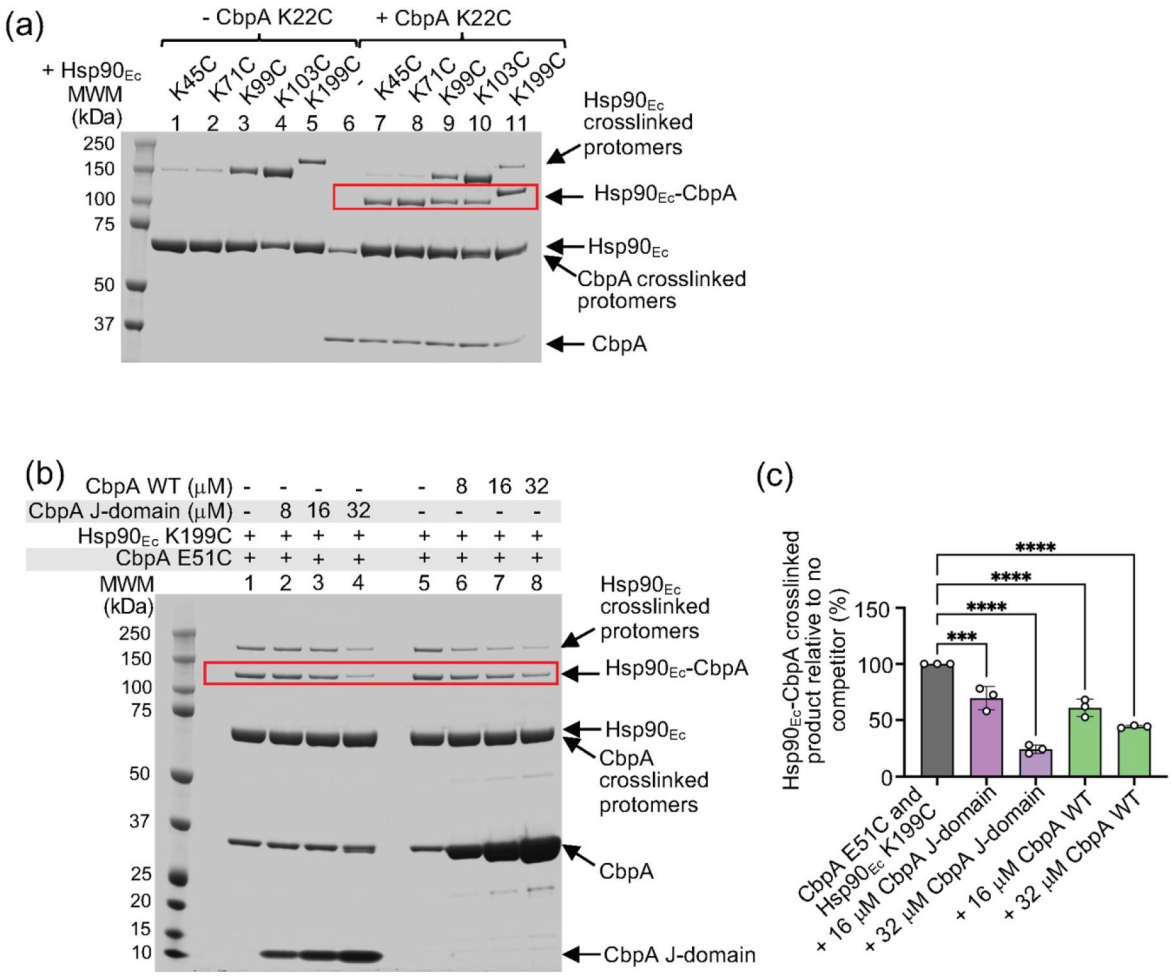

Figure 11. Interaction between the CbpA J-domain and $Hsp90_{Ec}$ NTD.

(a) BMOE crosslinking between CbpA and various $Hsp90_{Ec}$ NTD mutants. (b) BMOE crosslinking between CbpA E51C and $Hsp90_{Ec}$ N347C in the presence of increasing CbpA J-domain fragment or CbpA wild-type as described in Materials and Methods. In (a-b) $Hsp90_{Ec}$-CbpA crosslinked species are outlined with red boxes. Representative gels are shown of three replicates. (c) Quantification of CbpA-$Hsp90_{Ec}$ crosslinked species shown in (b). Means ±SD are shown. Crosslinking with CbpA J-domain or CbpA wild-type present is compared to control lane without CbpA J-domain or CbpA wild-type using one-way Anova, n = 3, *** 0.0001 < P < 0.001, ****P < 0.0001.

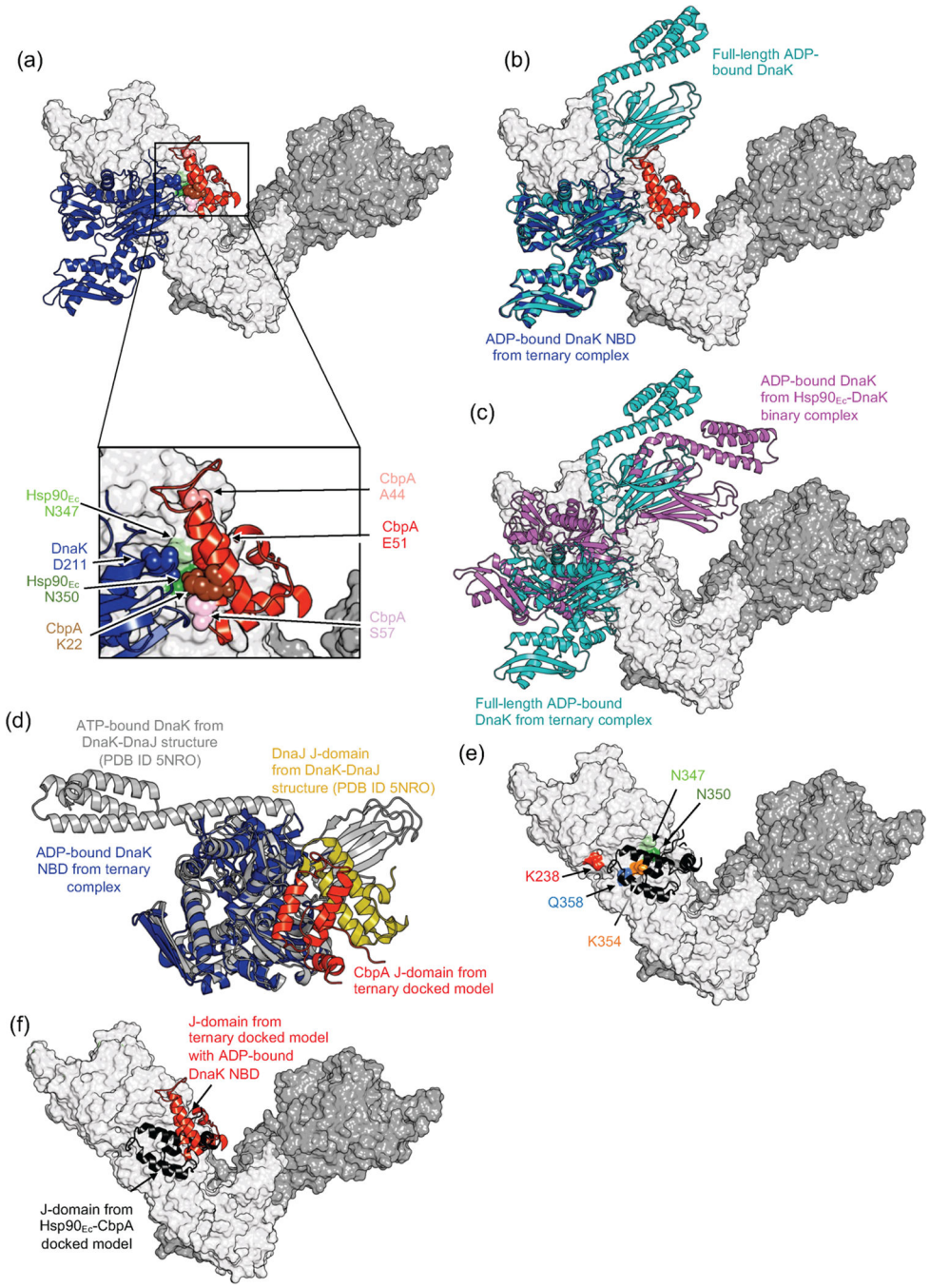

Figure 12. Docked models of the ternary $Hsp90_{Ec}$-DnaK-CbpA complex and binary $Hsp90_{Ec}$-CbpA complex.

(a) Top ranked docked model (cluster 1) of the $Hsp90_{Ec}$-DnaK-CbpA complex. Modeling was performed using the structures of the CbpA J-domain, the DnaK NBD in the ADP bound conformation and the apo form of one $Hsp90_{Ec}$ protomer, as described in Materials and Methods. The model was aligned with dimeric $Hsp90_{Ec}$. In the top ranked model $Hsp90_{Ec}$ is shown in surface representation with one protomer in white and the other protomer in grey. DnaK is shown in cartoon representation with the NBD in dark blue. The CbpA J-domain is shown in cartoon representation in red. The predicted interaction

interfaces are enlarged in the inset figure. Residues identified to participate in the interaction by crosslinking experiments are indicated with residue number. (b) Alignment of the full-length ADP-bound DnaK structure (PDB ID 2KHO), shown in cyan, with the DnaK NBD, shown in dark blue, in the $Hsp90_{Ec}$-DnaK-CbpA docked model in (a). (c) Comparison of full-length ADP-bound DnaK, in cyan, in the ternary $Hsp90_{Ec}$-DnaK-CbpA complex shown in (b) with DnaK from the binary $Hsp90_{Ec}$-DnaK docked model, in purple, that was generated previously [12]. $Hsp90_{Ec}$ molecules from the two models were aligned for the comparison. The CbpA J-domain from the ternary complex is omitted for clarity. (d) Comparison of the J-domain orientation relative to DnaK in the $Hsp90_{Ec}$-DnaK-CbpA ternary docked complex (showing the J-domain in red and DnaK NBD in dark blue) with the position of the J-domain in the DnaK-DnaJ J-domain co-crystal structure from PDB ID 5NRO [32] (showing J-domain in gold and DnaK in grey). $Hsp90_{Ec}$ from the ternary docked complex is omitted for clarity. The NBDs of DnaK were aligned for the comparison. (e) Docked model of the $Hsp90_{Ec}$ MD-CbpA J-domain complex generated as described in Materials and Methods. The J-domain is shown in black. $Hsp90_{Ec}$ interacting residues identified experimentally or by XL-MS are indicated by residue number. (f) Comparison of the J-domain interaction with the $Hsp90_{Ec}$ MD in the binary docked model shown in (e) (showing the J-domain in black) with the J-domain interaction with $Hsp90_{Ec}$ in the ternary docked model shown in (a) (showing the J-domain in red). $Hsp90_{Ec}$ molecules from the two models were aligned for the comparison. Protein structures were rendered in PyMOL.

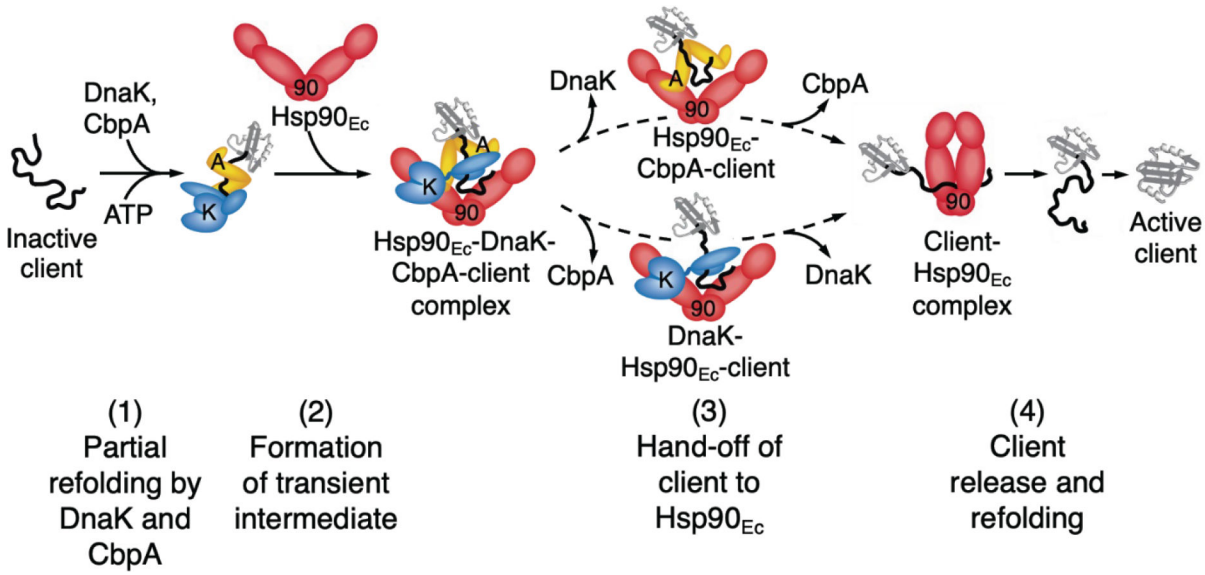

Figure 13. Working model for protein reactivation.

It is likely that DnaK binds the inactive client protein in a reaction stimulated by CbpA and promotes partial refolding of the client by repeated ATP-dependent cycles of client binding and release (1). DnaK and CbpA may interact transiently with the MD of $Hsp90_{Ec}$, forming an $Hsp90_{Ec}$-DnaK-CbpA complex with the client (2). Then the client is possibly transferred from DnaK to $Hsp90_{Ec}$ as DnaK and CbpA dissociate (3). Lastly, $Hsp90_{Ec}$ releases the client, which refolds in its active conformation (4). Many aspects of the working model are speculative and further investigation is required.